BBA - Molecular Basis of Disease 1870 (2024) 167479

Contents lists available at ScienceDirect

BBA - Molecular Basis of Disease

journal homepage: www.elsevier.com/locate/bbadis

25-Hydroxycholesterol attenuates tumor necrosis factor alpha-induced blood-brain barrier breakdown *in vitro*

Rodrigo Azevedo Loiola [a,1], Cindy Nguyen [a,1], Shiraz Dib [a], Julien Saint-Pol [a], Lucie Dehouck [a], Emmanuel Sevin [a], Marie Naudot [b], Christophe Landry [a], Jens Pahnke [c,d,e,f], Caroline Pot [g], Fabien Gosselet [a,*]

[a] *University of Artois, UR2465, Blood-Brain Barrier (BBB) Laboratory, F-62300 Lens, France*
[b] *Plateforme d'Ingénierie Cellulaire & Analyses des Protéines ICAP, FR CNRS 3085 ICP, Université de Picardie Jules Verne, F-80039 Amiens, France*
[c] *Translational Neurodegeneration Research and Neuropathology Lab, Department of Clinical Medicine (KlinMed), Medical Faculty, University of Oslo (UiO), Section of Neuropathology Research, Department of Pathology (PAT), Clinics for Laboratory Medicine (KLM), Oslo University Hospital (OUS), Sognsvannsveien 20, NO-0372 Oslo, Norway*
[d] *Institute of Nutritional Medicine (INUM)/Lübeck Institute of Dermatology (LIED), University of Lübeck (UzL), University Medical Center Schleswig-Holstein (UKSH), Ratzeburger Allee 160, D-23538 Lübeck, Germany*
[e] *Department of Pharmacology, Faculty of Medicine and Life Sciences, University of Latvia (LU), Jelgavas iela 3, LV-1004 Rīga, Latvia*
[f] *School of Neurobiology, Biochemistry and Biophysics, The Georg S. Wise Faculty of Life Sciences, Tel Aviv University (TAU), Ramat Aviv, IL-6997801, Israel*
[g] *Lausanne University Hospital (CHUV), University of Lausanne, Laboratories of Neuroimmunology, Service of Neurology and Neuroscience Research Center, Department of Clinical Neurosciences, CH-1011 Lausanne, Vaud, Switzerland*

A R T I C L E I N F O

Keywords:
Blood-brain barrier
Oxysterols
ABCA1
Inflammation
Brain pericytes
Vascular biology
25-hydroxycholesterol
TNFα
LXR
SREBP-2

A B S T R A C T

Intracellular cholesterol metabolism is regulated by the SREBP-2 and LXR signaling pathways. The effects of inflammation on these molecular mechanisms remain poorly studied, especially at the blood-brain barrier (BBB) level. Tumor necrosis factor α (TNFα) is a proinflammatory cytokine associated with BBB dysfunction. Therefore, the aim of our study was to investigate the effects of TNFα on BBB cholesterol metabolism, focusing on its underlying signaling pathways. Using a human *in vitro* BBB model composed of human brain-like endothelial cells (hBLECs) and brain pericytes (HBPs), we observed that TNFα increases BBB permeability by degrading the tight junction protein CLAUDIN-5 and activating stress signaling pathways in both cell types. TNFα also promotes cholesterol release and decreases cholesterol accumulation and APOE secretion. In hBLECs, the expression of SREBP-2 targets (LDLR and HMGCR) is increased, while ABCA1 expression is decreased. In HBPs, only LDLR and ABCA1 expression is increased. TNFα treatment also induces 25-hydroxycholesterol (25-HC) production, a cholesterol metabolite involved in the immune response and intracellular cholesterol metabolism. 25-HC pretreatment attenuates TNFα-induced BBB leakage and partially alleviates the effects of TNFα on ABCA1, LDLR, and HMGCR expression. Overall, our results suggest that TNFα favors cholesterol efflux *via* an LXR/ABCA1-independent mechanism at the BBB, while it activates the SREBP-2 pathway. Treatment with 25-HC partially reversed the effect of TNFα on the LXR/SREBP-2 pathways. Our study provides novel perspectives for better understanding cerebrovascular signaling events linked to BBB dysfunction and cholesterol metabolism in neuroinflammatory diseases.

1. Introduction

Cholesterol is the main component of the mammalian cell membrane and is a precursor for steroid hormone production, thus playing a pivotal role in several biological processes such as bilayer fluidity, membrane integrity, cell signaling and the regulation of the inflammatory response (1). In the central nervous system (CNS), cholesterol plays an essential role in myelin sheath formation, synaptogenesis, and membrane repair (2). The main source of CNS cholesterol is provided through *de novo* synthesis by astrocytes, since the exchange of cholesterol between the

* Corresponding author at: Blood-Brain Barrier Laboratory, Sciences Faculty Jean Perrin, Artois University, Lens, France.
E-mail address: fabien.gosselet@univ-artois.fr (F. Gosselet).
[1] Equal contribution.

https://doi.org/10.1016/j.bbadis.2024.167479
Received 24 May 2024; Received in revised form 5 August 2024; Accepted 20 August 2024
Available online 23 August 2024

brain and the periphery is highly restricted by the blood-brain barrier (BBB), a physical and metabolic barrier that isolates the brain from the bloodstream (3). Endothelial cells (ECs) that form a monolayer at the brain microvessel level are the central component of the BBB, and act as a physical barrier due to the presence of tight junctions (TJs) between adjacent ECs and the absence of fenestration and pinocytic activity (4,5). In addition, the delivery of essential nutrients to the brain parenchyma is strictly regulated by specific enzymes, receptors, and efflux pumps expressed on the apical side of BBB ECs (5,6). The specific features of BBB ECs are finely regulated by their interaction with perivascular structures, such as brain pericytes, the basal lamina, and astrocytic end-feet and neurons (7). The impaired communication among such components may result in BBB dysfunction, which is an underlying mechanism of the onset and progression of several neurodegenerative diseases (7). Although it is well accepted that BBB dysfunction is among the earliest events in neurodegenerative disorders, few studies have addressed strategies to understand the mechanisms underlying BBB impairment or proposed therapeutic interventions to prevent BBB dysfunction.

In parallel, it was suggested that an imbalance in CNS lipid homeostasis might be linked to the onset and progression of neurodegenerative disorders, such as Alzheimer's disease (AD) (8), Huntington's disease (9), Parkinson's disease (9), and multiple sclerosis (MS) (2). For example, in AD, very long-chain fatty acids are involved in peroxisomal dysfunctions, and phospholipid levels might constitute interesting biomarkers for detecting the disease at the prodromal stage (10). Furthermore, the expression levels of the CNS cholesterol transporter ABCA1 are closely associated with β-amyloid deposition in AD (11–13), and single polymorphisms of this gene have been recently linked to disease onset and progression (14). The expression of ABCA1 is tightly controlled by liver X receptors (LXRα and β) (15), therefore the LXR/ABCA1 axis represents a very promising therapeutic target for AD and other neurological disorders (16). Several studies have demonstrated that ABCA1 is the major cholesterol transporter involved in cholesterol release to apolipoproteins at the BBB and that its expression is regulated by the liver X receptor (LXR) pathway (17–19). On the other hand, the rate-limiting enzyme of cholesterol biosynthesis, 3-hydroxy-3-methylglutaryl-coenzyme A reductase (HMGCR), and the low-density lipoprotein receptor (LDLR), which is responsible for the lipoprotein uptake, are both regulated by the sterol response element-binding protein 2 (SREBP-2) pathway (20–23). In this way, the balance between LXR and SREBP-2 activation plays a key role on the regulation of cholesterol metabolism in the brain.

Despite the body of evidences highlighting the involvement of cholesterol on the CNS homeostasis and onset of brain diseases, the mechanisms underlying the associations among SREBP-2, LXR/ABCA1, and inflammation at the BBB level and its link with the onset and progression of neurological disorders are not fully understood. In recent years, oxysterols, a subset of oxidized cholesterol metabolites, including 24S-hydroxycholesterol (24S-HC) and 25-hydroxycholestherol (25-HC), have received increasing attention (10,24,25). Some of these oxysterols are LXR ligands and control ABCA1 expression (26). In particular, studies have highlighted the potential involvement of 25-HC. For instance, recent findings have demonstrated that 25-hydroxycholestherol (25-HC) inhibits SREBP-2 function and plays a key role in the regulation of inflammatory processes in the brain (reviewed in (26)). Further studies demonstrated that 25-HC levels increased in plasma of MS patients in a 5-year follow-up study (27) but is decreased in relapsing-remitting MS patients compared to controls (28). In parallel, Meffre et al. (2015) demonstrated that activation of LXR by 25-HC upregulated myelin expression and remyelination in organotypic cerebellar slice cultures (29). Moreover, the step-limiting enzyme responsible for 25-HC production, namely cholesterol 25 hydroxylase (CH25H), was found to be overexpressed in brains of AD patients, as well as in mouse models of β-amyloidosis deposition and tau-mediated neurodegeneration (30). Finally, 25-HC levels are increased in the brains tissue and cerebrospinal fluid (CSF) of late-stage AD patients (31).

Taken together, these previous findings strongly support a key role for 25-HC in CNS homeostasis, both in the regulation of brain cholesterol metabolism and in the control of neuroinflammatory processes (26). However, the interactions between TNFα, SREBP-2, the LXR/ABCA1 axis and 25-HC remain to be clarified, especially at the level of endothelial cells and pericytes of the BBB.

Therefore, the present study was designed to investigate the effects of inflammation on the cholesterol metabolism, with focus not only on BBB ECs but also on brain pericytes. For this purpose, we employed a well-established *in vitro* human BBB model consisting of $CD34^+$-derived endothelial cells cocultured with human brain pericytes (HBPs) to induce BBB properties (32). After induction of the BBB properties, the BBB ECs are named brain-like endothelial cells (hBLECs). Tumor necrosis factor α (TNFα) a proinflammatory cytokine with well-described involvement in chronic neurological disorders and BBB dysfunction (33–35), was used to induce an inflammatory response in the *in vitro* BBB model. Herein, we demonstrated first that TNFα induces BBB disruption *via* CLAUDIN-5 degradation and alters cholesterol metabolism at the hBLEC and HBP levels *via* activation of the SREBP-2 pathway. Secondly, our data suggested that TNFα increases 25-HC bioavailability. At last, pretreatment with 25-HC, which inhibits the SREBP-2 pathway, attenuated the TNFα-induced BBB breakdown. Overall, our study provides new evidence highlighting the potential role of oxysterols in the regulation of BBB homeostasis and pinpoints such molecules as promising therapeutic targets for treating neurodegenerative disorders.

2. Materials and methods

2.1. Reagents

Endothelial Cell Growth Medium MV2 (ECGMV2) and supplement (ref C22022) were purchased from PromoCell GmbH (Heidelberg, Germany), fetal bovine serum (FBS) from Thermo Fisher Scientific (Illkirch, France), and penicillin–streptomycin from ScienCell Research Laboratories Inc. (Carlsbad, CA, USA). Dulbecco's modified Eagle medium (DMEM), bovine serum albumin (ref A3311), TNFα (ref SRP3177), 25-HC (ref H1015), APOA-I (ref 178,452), HDL (ref 437,641), Interferon γ (IFNγ, ref. IF002), Matrigel™ (ref 354,230), the LXR inhibitor GSK2033 (ref SML1617), the SREBP inhibitor PF-429242 (ref SML0667), L-glutamine (ref G8540), and the LXR agonist T0901317 (ref T2320) were all purchased from Sigma-Aldrich (Merck KGaA, Saint-Quentin-Fallavier, France). Gentamycin sulfate (ref L0011–100) added to the PromoCell culture medium at 0.5 % was purchased from VWR International LLC (Radnor, PA, USA).

2.2. Cells

Human brain pericytes (HBPs) were kindly provided by Dr. Fumitaka Shimizu and Pr. Takashi Kanda from the Department of Neurology and Clinical Neuroscience, Graduate School of Medicine, Yamaguchi University, Ube, Japan. HBPs were isolated from a patient who had suddenly died from a heart attack (36). The study protocol for human tissue was approved by the ethics committee of the Medical Faculty (IRB#: H18–033-6), University of Yamaguchi Graduate School, and was conducted in accordance with the Declaration of Helsinki, as amended in Somerset West in 1996. For the $CD34^+$-hematopoietic stem cells, written informed consent was obtained from the family of the participant before enrollment in the study. The collection of human umbilical cord blood requires that infants' parents signed consent forms in compliance with French legislation. The protocol was approved by the French Ministry of Higher Education and Research (CODECOH, Number DC2011–1321). All experiments were carried out in accordance with the approved protocol. HBPs and $CD34^+$-hematopoietic stem cells were regularly checked for mycoplasma contamination, and short tandem repeat (STR) analysis confirmed the absence of cross-contamination. According to

French legislation, human cells were handled in the laboratory under agreement number L2–1235.

$CD34^+$-hematopoietic stem cells were isolated from human umbilical cord blood and differentiated into ECs ($CD34^+$-ECs) as previously described (37). $CD34^+$-ECs were seeded in 100 mm 1 % gelatin-coated dishes containing complete ECGMV2 supplemented with 0.5 % gentamicin. The HBPs were grown in DMEM supplemented with 4.5 g/L D-glucose, 10 % FBS, 1 % L-glutamine, and 1 % penicillin-streptomycin, as previously described (36).

2.3. In vitro BBB model with human brain-like endothelial cells (hBLECs)

The BBB model was reproduced as previously published (32,38). Briefly, $CD34^+$-ECs (8×10^4 cells/insert) were seeded into Matrigel™-coated filters (Costar Transwell inserts, pore size 0.4 μm, Corning SAS, Avon, France). Then, the inserts were placed in collagen-coated 12-well plates containing HBPs (5×10^4 cells/well). After 5 days of coculture, $CD34^+$-ECs acquire the major BBB properties observed *in vivo* and reproduce a suitable model to for investigating BBB permeability and physiology (39,40). These cells are therefore referred to as human brain-like ECs (hBLECs). HBPs were also deeply characterized in our previous studies (18,38,41). The upper compartment represents the apical side of the model (blood), and the lower side, represents the basolateral compartment (brain). Once differentiated, hBLECs were treated, and permeability studies and sample collection were subsequently performed as described below.

2.4. Treatments

All experiments were performed in the absence of serum or other commercial growth factors. All treatments were diluted in serum-free ECGMV2 containing 0.1 % BSA. For inflammatory conditions mimicking CNS inflammation, TNFα (1 and 10 ng/mL) or interferon γ (IFNγ, 1 and 10 ng/mL) were added to the basolateral compartment of the BBB model. For the coincubation of 25-HC with TNFα, 25-HC was added to the basolateral compartment 15 min prior to the addition of TNFα to the media. For the coincubation of T0901317 (10 μM), GSK2033 (1 μM) and PF-429242 (SREBP inhibitor, 1 μM) with TNFα, these compounds were added to both the basolateral and apical compartments 15 min before the TNFα treatment.

2.5. Permeability assay

Permeability assays were performed as previously described (42). Ringer–HEPES (RH buffer) buffer (150 mM NaCl, 5.2 mM KCl, 2.2 mM $CaCl_2$, 0.2 mM $MgCl_2$, 6 H_2O, 6 mM $NaHCO_3$, 5 mM HEPES, pH 7.4) at 37 °C was added to empty wells in a 12-well plate (Costar). Filter inserts containing hBLECs were subsequently transferred to a 12-well plate and filled with RH containing the fluorescent integrity marker sodium fluorescein (NaFlu; 10 μM; Life Technologies, Carlsbad, CA, USA), which poorly crosses the BBB. After 1 h, the filter inserts were withdrawn from the receiver compartment. Aliquots from the donor solution were taken at the beginning and end of the experiments, and the fluorescence was quantified using a microplate reader (Synergy H1 multiplate reader, BioTek Instruments SAS, Colmar, France) at an excitation wavelength (λ) of 490 nm and an emission wavelength of 525 nm. The permeability coefficient was then calculated as previously described (42). Briefly, both the insert permeability (PSf, for inserts only coated with Matrigel™) and the permeability of inserts containing hBLECs (PSt, for inserts with Matrigel™ and cells) were considered according to the following formula: $1/PSe = 1/PSt - 1/PSf$. The permeability value of the hBLEC monolayer was then divided by the surface area of the insert (1.12 cm^2) to obtain the permeability coefficient (Pe) of each molecule (at 10^{-3} cm/min).

2.6. Transendothelial electrical resistance (TEER) measurements

The resistance of the seeded or coated (empty) inserts was measured using an EVOM2 device (with a chopstick, World Precision Instruments, Friedberg, Germany) following the manufacturer's instructions and immediately after the inserts were removed from the incubator. For the calculation of the TEER values, the resistance of the coated inserts without cells was subtracted from the resistance obtained with cells and multiplied by the surface area of the insert (1.12 cm^2). TEER measurements were performed on triplicate inserts of two independent differentiations.

2.7. Toxicity and viability assays

Cell viability was evaluated by a WST-1 assay (Roche, Bâle, Switzerland), a water-soluble tetrazolium salt, according to the manufacturer's instructions. ATP levels in hBLECs and HBPs were measured with a luminescent kit (Merck KGaA) following the manufacturer's instructions. The lactate levels in the supernatant were measured using a homemade kit, as previously reported (43). Briefly, the supernatants were collected after treatment and frozen. Then, 10 μL of the supernatant was incubated with 90 μL of the lactate assay mixture, which was composed of 86 mM triethanolamine HCl, 8.6 mM EDTA.Na, 34 mM $MgCl_2.6H_2O$, 326 μM *N*-methylphenazonium methyl sulfate, 790 μM p-iodonitrotetrazolium violet, 7 % ethanol, 0.4 % Triton-X-100, 3.3 mM β-nicotinamide adenine dinucleotide and 4 U/mL lactate dehydrogenase. All reagents were purchased from Merck KGaA. After 9 min of incubation, the absorption was measured using a Synergy H1 microplate reader at 490 nm, and the lactate concentration in the supernatant was calculated according to a standard lactate curve.

Mitochondria activity of living cells was assessed by MTT cell proliferation assay. Briefly, after 24 h treatment with 10 ng/mL TNFα +/− 10 μM 25-HC, cell medium was changed with complete medium supplemented with 1 mg/mL 3-(4,5-Dimethyl-2-thiazolyl)-2,5-diphenyl-2H-tetrazolium Bromide (MTT, ref. 475,989, Sigma-Aldrich) for 1 h. MTT medium was then removed, and intracellular formazan crystals were dissolved in pure DMSO to measure the absorbance at 570 and 630 nm for cell proliferation rate and background subtraction respectively. To allow the cell proliferation evaluation, cells were previously counted to refer to the precise number of cells per well.

2.8. Immunofluorescence and confocal analysis

hBLECs were fixed with ice-cold methanol (20 s) for CLAUDIN-5 labeling or cold paraformaldehyde (PFA) 4 % (10 min) for the other targets and rinsed twice with cold calcium and magnesium free PBS (PBS-CMF; 8 g/L NaCl, 0.2 g/L KCl, 0.2 g/L KH_2PO_4, 2.86 g/L $Na_2HPO_4{\cdot}12\,H_2O$; pH 7.4). A step of 10 min-permeabilization (10 min at room temperature (RT)) with 0.1 % Triton X-100 in PBS-CMF was required for PFA-fixed samples. For the colabelling of CLAUDIN-5 and endomembrane markers (RAB7A and HSP90B1), cells were fixed with cold PFA (2 %). Unspecific binding was blocked (30 min, RT) using a sea block buffer solution (SBBS, Thermo Fisher Scientific). Then, the cells were incubated (60 min, RT) with primary antibodies against CLAUDIN-5 (1:100, Invitrogen, 34–1600), ZO-1 (1:200, Invitrogen, 61–7300), VE-CADHERIN (1:400, Abcam, Ab33168), RAB7A (1:100, Cell Signaling, 95746S), HSP90B1 (1:100, Sigma-Aldrich, AMAB91019) and Ki-67 (1:200, Abcam, Ab16667) in PBS-CMF containing 5 % (*v*/v) SBBS (PBS-SBBS). After rinsing, the cells were incubated (30 min, RT) with a secondary polyclonal antibody (Life Technologies, A-11034) and 10 ng/mL DAPI (Invitrogen, D1306) for nuclear staining in PBS-SBBS. For F-ACTIN staining, the cells were incubated (30 min, RT) with phalloidin (1:40, Bodipy – 588/568 – Thermo Fisher Scientific, B3475) during the secondary antibody step. After rising, the cells were mounted using ProLong Gold Antifade Mountant (Thermo Fisher Scientific). Images were acquired using a Leica microscope (DMi8, Leica Microsystems SAS,

Nanterre, France) and processed using ImageJ software (National Institutes of Health, Bethesda, MD, USA).

For Ki-67 labelling, HBPs were then analyzed using ImageJ and results were reported to the total number of nuclei per condition.

Confocal analysis was made using the confocal microscope LSM780 (Zeiss, Oberkochen, Germany). Pearson's correlation coefficient were then calculated using 10 fields per condition in 3 independent experiments.

2.9. FACS-like Ki-67 positive cell measurement

Non-treated and treated cells were rinsed twice with PBS-CMF, and then resuspended in Accutase® (Sigma-Aldrich) at 37 °C, 5 % CO_2. After 10 min, action of Accutase® was stopped by the addition of complete medium. Cells were then counted, and 2.5 to 3 × 10^6 cells were then processed for Ki-67 immunostaining. Briefly, suspended cells were fixed 10 min in 4 % PFA and permeabilized in PBS-CMF/0,1 % Saponin (PBS-S). Cells were then saturated in SBB solution/0,1 % Saponin and labeled with Anti-Ki-67 antibody (same reference used in IF) in PBS-S 2 % SBB for 1 h on a rotary agitator. After 3 cycles of washing in PBS-S/pelleting at 1000 ×*g* for 5 min, cells were labeled with secondary goat anti-Rabbit AF488 (Thermo Fisher Scientific) in PBS-S 2 % SBB for 1 h on a rotary agitator. After 3 cycles of washing in PBS-S/pelleting at 1000 ×*g* for 5 min, the fluorescence was measured using a Synergy H1 multiplate reader (Ex: 475 nm, Em: 509 nm). Results were reported to the cell number initially counted.

2.10. RT-qPCR

After treatment, mRNA from hBLECs and HBPs were extracted using a NucleoSpin® RNA/protein kit (Macherey-Nagel, Dueren, Germany). cDNA were obtained from 250 ng of mRNA using IScript™ Reverse Transcription Supermix (Bio-Rad, Hercules, CA, USA), following the manufacturer's instructions. For *CYP7B1* mRNA expression in hBLECs, cDNA were obtained from 250 ng to 1 µg of mRNA, but no signal was detected. qPCR reactions (10 µL) were prepared using SsoFast™ EvaGreen® Supermix (Bio-Rad), primers (100 nM), deionized water, and cDNA. qPCR amplification was carried out for 40 cycles with an annealing temperature of 60 °C in a CFX96 thermocycler (Bio-Rad). Ct data were obtained using Bio-Rad CFX Manager software. Gene expression levels of the targets (please see Table 1) were calculated using the $2^{-\Delta\Delta Ct}$ method relative to the housekeeping gene glyceraldehyde 3-phosphate dehydrogenase (*GAPDH*). The specificity and efficiency of all the target genes primers were evaluated before performing qPCR.

Table 1
Primers sequences for qPCR. Primer pairs: F: forward primer and R: reverse primer.

Target	Sequence (F/R)	Accession Number
ABCA1	F: CAGTGCTTCCTGATTAGCACAC R: AGGCTAGCGAAGATCTTGGTG	NM_005502.4
APOE	F: GGTCGCTTTTGGGATTACCT R: CCTTCAACTCCTTCATGGTCTC	NM_001302690.2
CH25H	F: ACATCTGGCTTTCCGTGGAG R: TACGGAGCGAAGTTGCAGTT	NM_003956.4
CYP7B1	F: GGCCCTCTGCTTGCTTGT R: AAGTTCAGGACCACTCCAAGAT	AH010394.2
HMGCR	F: TGTGTGTGGGACCGTAATGG R: GCTGTCTTCTTGGTGCAAGC	NM_001130996.2
LDLR	F: TTCATGGCTTCATGTACTGGAC R: TTTTCAGTCACCAGCGAGTAGA	NM_000527.5
LXRα (NR1H3)	F: CAGGGCCATGAATGAGCTGC R: TGTGCTGCAGCCTCTCTACC	NM_005693.4
LXRβ (NR1H2)	F: TCCTACCACGAGTTCCCTGG R: TGGTTCCTCTTCGGGATCTGG	NM_007121.7
GAPDH	F: GATGACATCAAGAAGGTGGTGA R: GCTGTTGAAGTCAGAGGAGACC	NM_001357943.2

2.11. Western blotting (WB)

Cells were collected with RIPA lysis buffer containing protease and phosphatase inhibitors (Sigma-Aldrich). Cell lysates (10–20 µg) were prepared, separated by sodium dodecyl sulfate-polyacrylamide gel electrophoresis (SDS-PAGE) and then transferred to nitrocellulose membranes (GE Healthcare, Little Chalfont, UK). Nonspecific binding was blocked using Tris-buffered saline containing 0.1 % Tween 20 (TBS-T) with 5 % skim milk (1 h, RT). The membranes were incubated (4 °C, overnight) with primary antibodies (Table 2), washed extensively, and then incubated (1 h, RT) with a horseradish peroxidase-conjugated secondary antibody (Dako, Lostrup, Denmark). After rinsing, the membranes were developed with a chemiluminescence reagent (GE Healthcare), and images were acquired using the Azure c600 WB Imaging System (Azure Biosystems, Dublin, Ireland). TotalLab TL 100 1D gel analysis software was used for quantification of the relative immunoblot densities (Gosforth, UK). For APOE detection, supernatants were collected, centrifuged, and stored at −20 °C. Soluble proteins were precipitated by diluting the supernatants (1:5 *v/v*) with pure acetone (Sigma Aldrich) followed by overnight incubation at −20 °C. Then, the samples were centrifuged (14,000 rpm for 10 min), and the supernatant was discarded. The remaining acetone air-dried pellet was resuspended in RIPA lysis buffer (Sigma-Aldrich) supplemented with anti-proteases and anti-phosphatases (Sigma-Aldrich). A BCA assay (Sigma-Aldrich) was performed for protein quantification, and immunoblotting was performed as described above. The immunoblots of APOE were then normalized by staining the membranes with Red Ponceau (Thermo Fisher Scientific) as previously described (18,44).

2.12. Cellular cholesterol efflux assay

To prepare the radiolabeled medium, 0.5 µCi/mL [^{3}H]-cholesterol (Perkin Elmer, Waltham, MA, USA) was added to the FCS of the ECGMV2 supplement and incubated at 37 °C for 3 h. Then, radiolabeled serum was added to ECGMV2 to prepare complete medium for the *in vitro* BBB model. The cells were maintained for 24 h in radiolabeled complete medium to promote the uptake of radiolabeled cholesterol by hBLECs and HBPs. Afterwards, the cells were rinsed twice with basal ECGMV2 medium and incubated with basal ECGMV2 medium supplemented with 0.1 % BSA in the absence or presence of 10 ng/mL TNFα or the LXR agonist T0901317 (10 µM). After 24 h of treatment, the cells were rinsed once with ECGMV2 + 0.1 % BSA and incubated for 4 h with ECGMV2 + 0.1 % BSA containing 50 µg/mL of high-density lipoproteins (HDL) or 20 µg/mL of apolipoprotein A-I (APOA-I). After incubation with the lipid acceptors, the supernatants were collected, and the hBLECs and HBPs were rinsed 4 times with cold RH buffer before being lysed with 1 % Triton X-100 (Sigma Aldrich). The supernatants and cell lysates were then centrifuged (4 min at 4000 rpm), and the radioactivity was quantified using an HIDEX 300SL scintillation counter (Sciencetec,

Table 2
Antibodies used for the immunoblot experiments.

Target	References and providers	Antibody dilution
ABCA1	ab18180 (Abcam)	1/500
CLAUDIN-5	GTX49370 (Genetex)	1/1000
COX2	AF4198 (R&D system)	1/1000
HMGCR	AMAB90619 (Sigma)	1/1000
ICAM-1	ab53013 (Abcam)	1/2000
LDLR	ab52818 (Abcam)	1/1000
NLRP3	ab263899 (Abcam)	1/1000
APOE	ab1906 (Abcam)	1/1000
CYP7B1	TA807549 (Origene)	1/1000
CH25H	ABS562 (Merck)	1/1000
VCAM-1	PA5-80213 (Thermo Fisher)	1/1000
ACTIN	A5441 (Sigma)	1/10000

Villebon-sur-Yvette, France). The intracellular cholesterol content was determined by measuring the disintegration per minute in the cell lysates. The relative cholesterol efflux was calculated as we previously described (17,18) according to the following formula:

Relative Cholesterol Efflux (%) = (Supernatant radioactivity [Bq]* 100)/(Supernatant radioactivity [Bq] + Lysate radioactivity [Bq]).

2.13. Dosage of total cell cholesterol

Cells of the human BBB model were treated with vehicule (ECGMV2 supplemented with 0.1 % BSA) or with 10 ng/mL of TNFα for 24 h. hBLECs and HBPs were then rinsed twice with RH buffer and resuspended in Accutase® for 10 min at 37 °C 5 % CO_2. Cells were then rinsed and pelleted 3 times in PBS-CMF at 300 ×*g* for 5 min at 4 °C. To extract the lipids, pellets were then lysed in chloroform/isopropanol/NP-40 (7:11:0.1, *v*/v) and lysates were centrifuged for 10 min at 13,000 ×*g* at room temperature. Supernatants were heated at 50 °C for 20 min and were subsequently dried in the vacuum for 30 min (rotavapor, Thermo Fisher Scientific). The samples were then assayed using a Cholesterol Quantitative Kit (Sigma-Aldrich, MAK043). Briefly, this assay uses a coupled enzyme giving a colorimetric (570 nm)/fluorometric (λex = 535 nm/λem = 587 nm) product, proportional to total cell cholesterol and more precisely free cholesterol and cholesteryl esters. Briefly, dried lipids were resuspended and sonicated in Cholesterol Assay Buffer and 50 μL per condition were incubated with 50 μL of reaction mix (22v. Cholesterol Assay Buffer, 1v. Cholesterol Probe, 1v. Cholesterol Enzyme Mix and 1v. Cholesterol esterase) for 1 h at 37 °C, 5 % CO_2. Total cholesterol per condition was quantified at 570 nm, and reported to the total quantity of proteins dosed by the Bradford protocol. The measurement of the total cell cholesterol was normalized by μg of proteins in each hBLEC and HBP sample.

2.14. Oxysterol extraction and 25-HC analysis by LC-MS/MS

To generate enough materials to dose the oxysterols, the human BBB model was set up in dishes of 100 mm diameter (Corning). Two days after thawing and growth in petri dishes, 6.25×10^5 HBPs were seeded in 100 mm dishes coated with rat tail collagen (type I) (BD Biosciences, Franklin Lakes, NJ, USA), cultured in ECGMV2 supplemented with supplement mix, and 0.5 % gentamicin and kept for 3 h at 37 °C as described above. Then, 3.1×10^6 $CD34^+$-derived ECs were seeded on 0.4 μm transwell inserts (Corning ref. 7910) coated with diluted 1/48 (*v*/v) Matrigel™. HBPs and ECs were cultured together for 6 days in a humidified 5 % CO_2 atmosphere to induce the hBLEC phenotype as described above. The medium was renewed every 2 days.

Then, TNFα or IFNγ (resuspended in basal ECGMV2 supplemented with 0.1 % BSA) was added to the abluminal compartment of the BBB model at a concentration of 10 ng/mL for 24 h. Then, oxysterol extraction from the medium was performed using methanol (CH_3OH), chloroform ($CHCl_3$) and 2,6-ditertiarybutyl-4-methylphenol (BHT) according to method of Bligh and Dyer (45). To summarize, 4 mL of 5 μM CH_3OH/BHT (1:0,09, *v*/v) was added to 2 mL of culture media. Then, 2 mL of $CHCl_3$ was added to each sample. The mixture was shaken vigorously for 30 min and then centrifuged for 10 min at 1200 rpm. The $CHCl_3$ fraction was recovered, and the process was repeated. $CHCl_3$ fractions were pooled and evaporated using rotavapor. The samples were stored at −80 °C until analysis.

For oxysterol extraction from cell lysates, cell lysis was performed with 4 mL of 5 μM CH_3OH/BHT (1:0.09, v/v) and 2 mL of water was added after cell scraping. The samples were frozen at −80 °C overnight and then sonicated for 30 min. The samples were treated as described above.

Analysis of 25-HC was performed using a quadrupole time-of-flight Triple TOF 5600 + mass spectrometer with electrospray ionization interface (ESI) coupled with an Eksigent Ekspert nanoLC 425 system (Sciex, Redwood City, USA). Five μL of standards or samples were injected into an Eksigent Halo C18 column (50 × 0.5 mm; 2.7 μm, 90 A). Samples were diluted in methanol/water/formic acid (20:80:0.1).

A multistep solvent gradient applied was set to 0 min at 20 % B; 3 min 20 % B; 4.5 min 80 % B and was held at 80 % up to 7.5 min where solvent A was water, 0.1 % formic acid and solvent B was methanol, 0.1 % formic acid. Flow rate was set to 10 μL/min. The column temperature was set to 25 °C. Mass spectrometer parameters were previously described by Madlen Reinicke et al. (46). Briefly, precursor ion was *m/z* 385.3 [M + H - H2O]+, quantifier ion was *m/z* 367.3 and qualifier ion was *m/z* 147.1. Source temperature was set to 300 °C, Ionspray Voltage set to 5500 V, Collision Energy to 30 V and Declustering Potential set to 100 V. Nebulizing gas and curtain gas were set to 20 and 10 psi respectively. External calibration curve was redone every 20 samples and shown linearity from 1 nM to 500 nM with a retention time at 3.8 min for 25-HC. Representative chromatograms and mass spectrum of 25-HC are shown in Supplementary Fig. 1.

2.15. Statistical analysis

The number of independent experiments for each figure is indicated by "n" in figure legends. All data were analyzed using GraphPad Prism® software version 8.0 (Dotmatics, Boston, MA, USA). The normality of continuous variables was assessed using the Shapiro-Wilk test ($n < 30$) or Kolmogorov-Smirnov test ($n > 30$). For variables that were not normally distributed, Mann-Whitney or Kruskall-Wallis tests were performed and the values are expressed as medians (interquartile ranges, 25–75). For variables that were normally distributed, Student's *t*-test or one-way ANOVA was performed, and the values ware expressed as the mean ± standard deviation (SD). The thresholds for statistical significance were set as $p < 0.05$ (*), $p < 0.01$ (**) and $p < 0.001$ (***) compared with the control (or untreated) conditions, or with the other treated conditions for Figs. 7 and 9.

3. Results

3.1. TNFα triggers inflammation in cells of the human blood-brain barrier (BBB) and promotes BBB opening

To understand the effect of TNFα from the cerebral compartment on the BBB, the *in vitro* model was exposed to two concentrations of TNFα (1 and 10 ng/mL) in the basolateral (corresponding to brain) compartment, followed by a time-curve evaluation of BBB features (4–48 h). TNFα quickly induces a stress response at the level of hBLECs and HBPs since the upregulation of inflammatory markers is quickly observed (Fig. 1). The inflammasome molecule NOD-like receptor family, pyrin domain-containing 3 (NLRP3, Fig. 1A), vascular cell adhesion molecule-1 (VCAM-1, Fig. 1B), and intercellular adhesion molecule 1 (ICAM-1, Fig. 1C) were significantly upregulated in hBLECs after 4, 8, 24 and 48 h of treatment with various concentrations of TNFα. Similar results were observed for HBPs (Fig. 1D), confirming that the inflammatory process is induced by TNFα in both cell types of the human BBB model.

We then investigated the effects of TNFα on BBB permeability and observed the TNFα-induced BBB disruption started after 8 h of treatment, as highlighted by a marked increase of the permeability to sodium fluorescein (NaFluo), a small paracellular fluorescent marker (Fig. 2A)

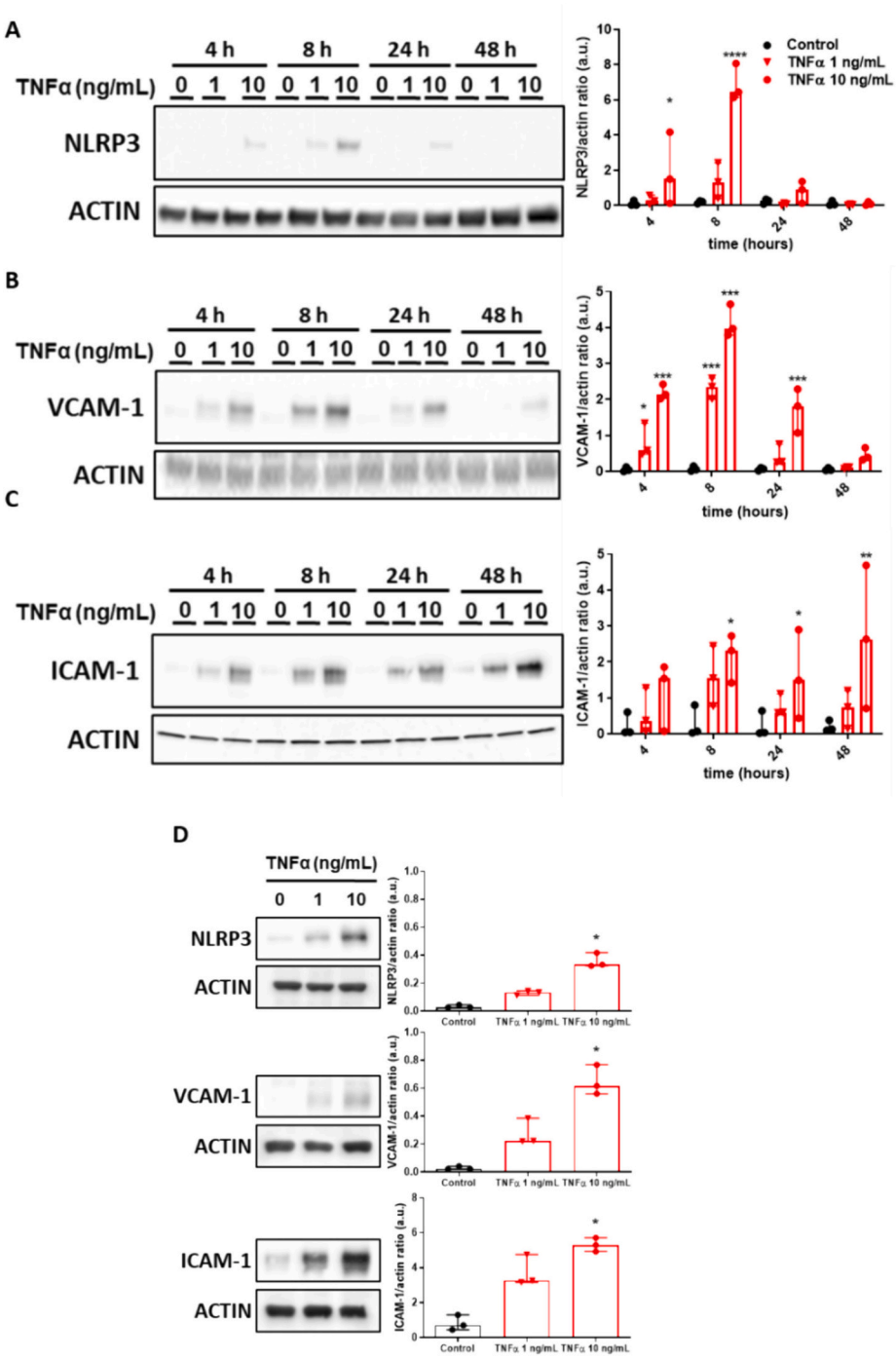

Fig. 1. Time- and concentration- dependent effects of TNFα on the expression of inflammatory markers in hBLECs and HBPs. Western blotting was performed on cell lysates from the *in vitro* BBB model treated for 4, 8, 24 or 48 h with 1 or 10 ng/mL TNFα to detect the protein expression of the inflammasome NRLP3 (A), adhesion molecule VCAM-1 (B) and intercellular adhesion molecule 1 (ICAM-1) in hBLECs. (D) NLRP3, VCAM-1 and ICAM-1 expression in HBPs after 24 h of treatment with 10 ng/mL TNFα. The data are presented as medians with interquartile ranges ($n = 3$).

and a decrease of the trans-endothelial electrical resistance (TEER) (Fig. 2B).

BBB disruption was more evident after 24 and 48 h of treatment, when 10 ng/mL TNFα was able to further increase the BBB permeability. In addition, even 1 ng/mL TNFα induced BBB breakdown after 24 and 48 h, but to a lesser extent than 10 ng/mL TNFα. We therefore chose to use 24 h and the 10 ng/mL TNFα concentration for subsequent experiments in our study. The TNFα-induced BBB breakdown was further confirmed by immunofluorescence analysis, that revealed that TNFα-treated cells presented disabled junction proteins, such as CLAUDIN-5, ZO-1, and VE-CADHERIN (Fig. 2C). Cell border presence of these junction proteins is disturbed (white arrows) whereas cytosolic presence is increased, thus suggesting location changes of these proteins, particularly CLAUDIN-5 that is an essential component for BBB integrity (47). To further investigate the effect of TNFα on TJ localization, a co-staining of claudin 5 and RAB7A (late endosomal marker) or HSP90B1 (endoplasmic reticulum marker) was performed. We then adapted our immunofluorescence protocol to focus on intracellular CLAUDIN-5 localization after TNFα treatment and observed that CLAUDIN-5 signal superposes with RAB7A but not with HSP90B1 (Fig. 2D). It is well-

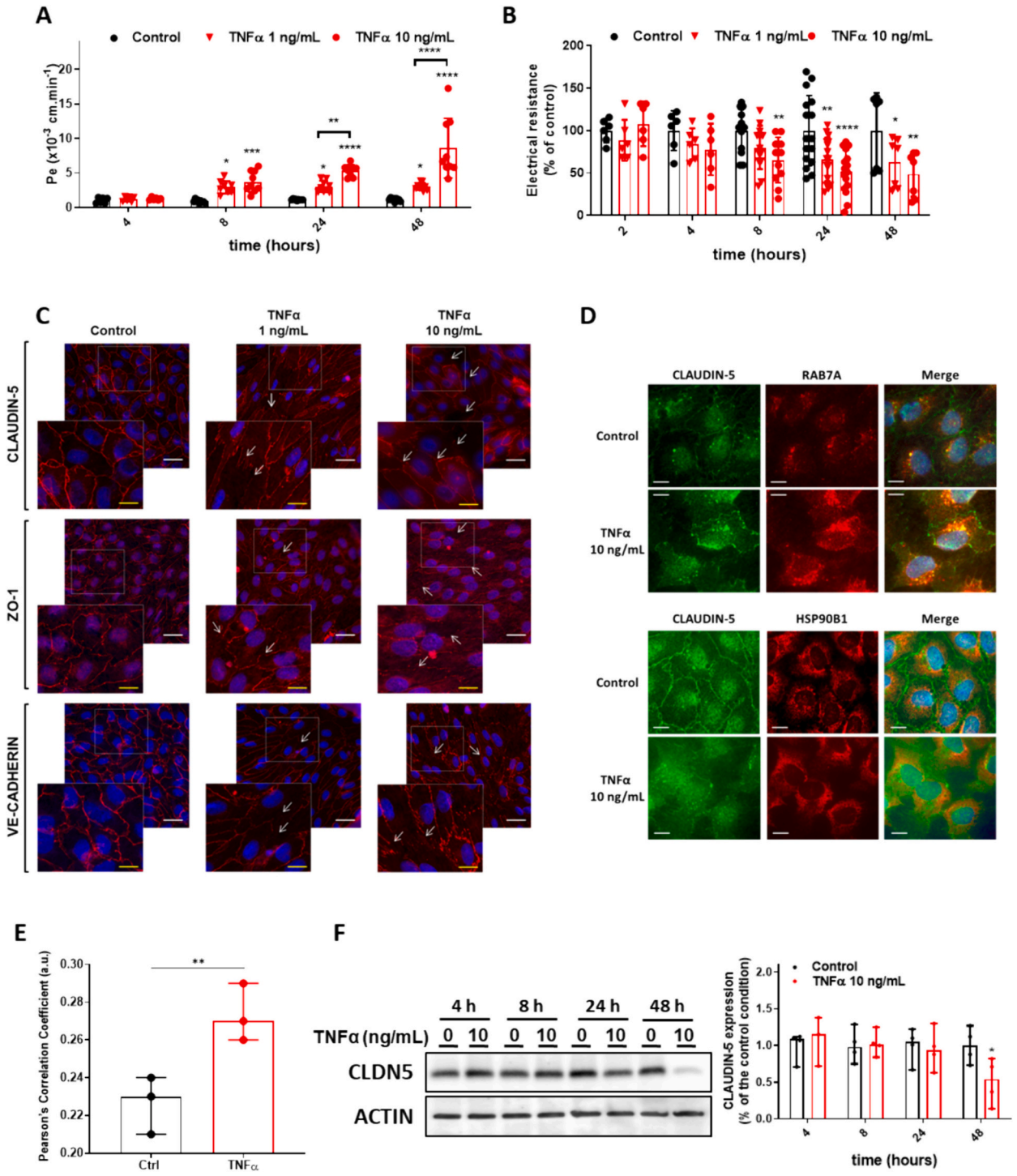

Fig. 2. Effect of the addition of 1 or 10 ng/mL TNFα to the basolateral compartment on the tightness of the human *in vitro* BBB model. Time-curve response of TNFα on paracellular permeability to the fluorescent marker sodium fluorescein (NaFlu) (A) or relative transendothelial electric resistance (TEER) (in %) (B). The basal TEER was 80.4 ± 6.8 Ω.cm^2. The data are presented as means ± SDs, $n = 6$–16. C, Representative images and magnifications of immunofluorescence staining for the detection and localization of tight junction (CLAUDIN-5 and ZO-1) and adherens junction (VE-CADHERIN) proteins following 24 h of treatment with 1 or 10 ng/mL TNFα. White scale bar: 10 μm, yellow scale bar: 5 μm. Loss of cell border cohesion was shown by white arrows. The immunofluorescence protocol was then adapted to investigate the intracellular location of the tight junction protein CLAUDIN-5 (in green) within hBLECs after 24 h of treatment with DMSO (control) or 10 ng/mL TNFα (D). RAB7A, a marker of late endosomes, was stained in red and nuclei were labeled with 10 ng/mL DAPI (blue). The pictures are representative of three independent experiments. Scale bar: 2.5 μm. (E) Calculation of Pearson's correlation coefficient from confocal pictures shows an increase of CLAUDIN-5 and RAB7A colocalization after 24 h of TNFα treatment. (F) Protein levels of CLAUDIN-5 were decreased 48 h after TNFα treatment. For (E) and (F), data are presented as medians with interquartiles, $n = 3$. (For interpretation of the references to colour in this figure legend, the reader is referred to the web version of this article.)

described that RAB7A-positive late endosomes will then fuse with lysosomes (48), suggesting that it will likely lead to CLAUDIN-5 degradation. We therefore performed confocal analysis of CLDN5-RAB7A colocalization and assessed CLDN5 protein expression after TNFα-treatment. We observed a significant increase of Pearson's correlation of CLDN5-RAB7A colocalization at 24 h after TNFα treatment (Fig. 2E) and a significant decrease of CLDN5 protein level at 48 h (Fig. 2F). Taken together, these results suggest that TNFα disrupts the tight junctions of the hBLEC monolayer and promotes the translocation of CLAUDIN-5 to the late endosomes to be subsequently degraded by the lysosomal system.

Furthermore, we evaluated the effect of TNFα on cell viability to identify putative toxic effects at the BBB level. TNFα (10 ng/mL) slightly decreased hBLEC viability (Fig. 3A) and ATP content (Fig. 3B) and increased lactate production (Supplementary Fig. 2), while 1 ng/mL TNFα had no effect. Interestingly, TNFα had no effect on HBP viability and ATP production at any tested concentration, suggesting that HBPs are less sensitive to the deleterious effects of TNFα than are hBLECs.

3.2. TNFα modulates cholesterol metabolism in cells of the human BBB model

To determine whether TNFα modulates cellular cholesterol metabolism, we analyzed the mRNA and protein expression of key players involved in cholesterol release (ABCA1 and APOE), cholesterol synthesis (HMGCR) and cholesterol uptake (LDLR).

Surprisingly, 10 ng/mL TNFα downregulated the mRNA and protein expression of ABCA1 in hBLECs, but upregulated ABCA1 expression in HBPs (Fig. 4A and B). However, 1 ng/mL TNFα, which had a mild effect on BBB permeability and did not induce hBLEC toxicity, had no effect on ABCA1 expression. Because ABCA1 expression is regulated by LXRα and LXRβ, we measured the mRNA expression of these nuclear receptors after TNFα treatment. LXRα is highly expressed in hBLECs and in HBPs when compared with LXRβ (Supplementary Fig. 3) and TNFα downregulates LXRα expression in hBLECs and upregulates LXRβ expression in HBPs (Fig. 4C). We can therefore hypothesize that TNFα differentially modulate LXRα and LXRβ expression in hBLECs and HBPs that subsequently might lead to different regulation of the ABCA1 expression in these two cell types.

Other ABC transporters (ABCG1, ABCG4, and ABCA7) known as cholesterol transporters were also investigated but TNFα had no effect on their protein expression (Supplementary Fig. 4). RT-qPCR analysis of *APOE* mRNA showed downregulation 24 h after treatment with TNFα 10 ng/mL in hBLECs (Fig. 4A) and this result was confirmed by analysis of cell supernatants from the basolateral compartment (brain) of the human BBB model (Fig. 4D). Interestingly, we were not able to detect any secretion of APOE protein on the apical side of the model (blood). TNFα upregulated the expression of LDLR in hBLECs and HBPs (Fig. 4A and E) and increased the expression of HMGCR only in hBLECs (Fig. 4A and E). Taken together, our results suggest that TNFα treatment modulates the levels of proteins involved in cholesterol efflux, production and uptake.

To further investigate the effect of 10 ng/mL TNFα on cholesterol metabolism, we evaluated the effect of TNFα treatment for 24 h on cholesterol efflux. For this purpose, we used two different cholesterol acceptors, namely, APOA-I and HDL. In addition, T0901317, a potent agonist of the LXR signaling pathway that controls ABCA1 expression, was used as a positive control for LXR activation and cholesterol efflux (17,18,49). As shown in Figs. 5A and B, 10 ng/mL TNFα increased cholesterol efflux to both acceptors (APOA-1 and HDL) only in hBLECs, and reduced the intracellular cholesterol content in hBLECs (Fig. 5C and D). These latter results were confirmed by analysis of total cellular cholesterol content using a dosage cholesterol kit as we performed in our previous study (41). Fig. 5E and F confirm that treatment of cells with 10 ng/mL of TNFα decreases the total cholesterol concentration in hBLECs, but not in HBPs.

Interestingly, increased cholesterol efflux was observed in both compartments of the human BBB model. These results were unexpected since ABCA1, the major cholesterol transporter involved in APOA-I and HDL efflux, was downregulated in hBLECs after TNFα treatment (Fig. 4A and B). The results observed after T0901317 (10 μM) treatment confirmed that activation of the LXR signaling pathway leads to cholesterol efflux. No changes in cholesterol efflux were detected in HBPs treated with TNFα, while T0901317 increased cholesterol efflux, suggesting that TNFα triggers a different cellular response in HBPs than in hBLECs. Taken together, these results suggest that the increase in cholesterol efflux observed in hBLECs after TNFα treatment is not mediated by the LXR/ABCA1 axis. Despite alterations in LDLR and ABCA1 expression, no cholesterol efflux is triggered in HBPs. Given we have observed a significant upregulation of LDLR and HMGCR in HBPs and hBLECs after TNFα treatment, we hypothesize that TNFα is a potent activator of the SREBP-2 pathway.

3.3. The 25-HC concentration in increased by TNFα

Since there is no evidence in the literature showing a direct effect of TNFα on LXR/SREBP-2 pathways in hBLECs and HBPs, we investigated whether TNFα-mediated BBB disruption could involve the regulation of 25-HC availability, which modulates the activity of these pathways. Indeed, several studies have demonstrated that 25-HC is a potent LXR agonist and inhibits the SREBP-2 pathway by sequestering SREBP proteins into the endoplasmic reticulum (26). Cholesterol is converted to 25-HC by cholesterol 25 hydroxylase (CH25H) (Fig. 6A). Afterwards, 25-HC can be subsequently converted by the enzyme CYP7B1 to 7α,25-dihydroxycholesterol (7α,25-DHC), an agonist of Epstein-Barr receptor 2 (EBI2), which elicits a strong inflammatory response. Therefore, we investigated the effect of TNFα on the expression of enzymes involved in the production of 25-HC (CH25H) and the oxidation of 25-HC to 7α,25-

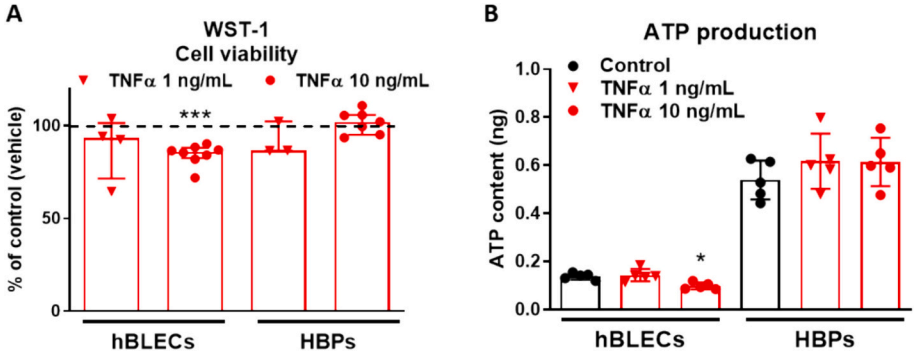

Fig. 3. Toxicity of TNFα (1 or 10 ng/mL for 24 h) on hBLECs and HBPs. TNFα effect on hBLECs and HBPs was assessed by a WST-1 assay (A) and ATP content in cell lysates (B). The data are presented as medians with interquartile ranges (n = 3–8).

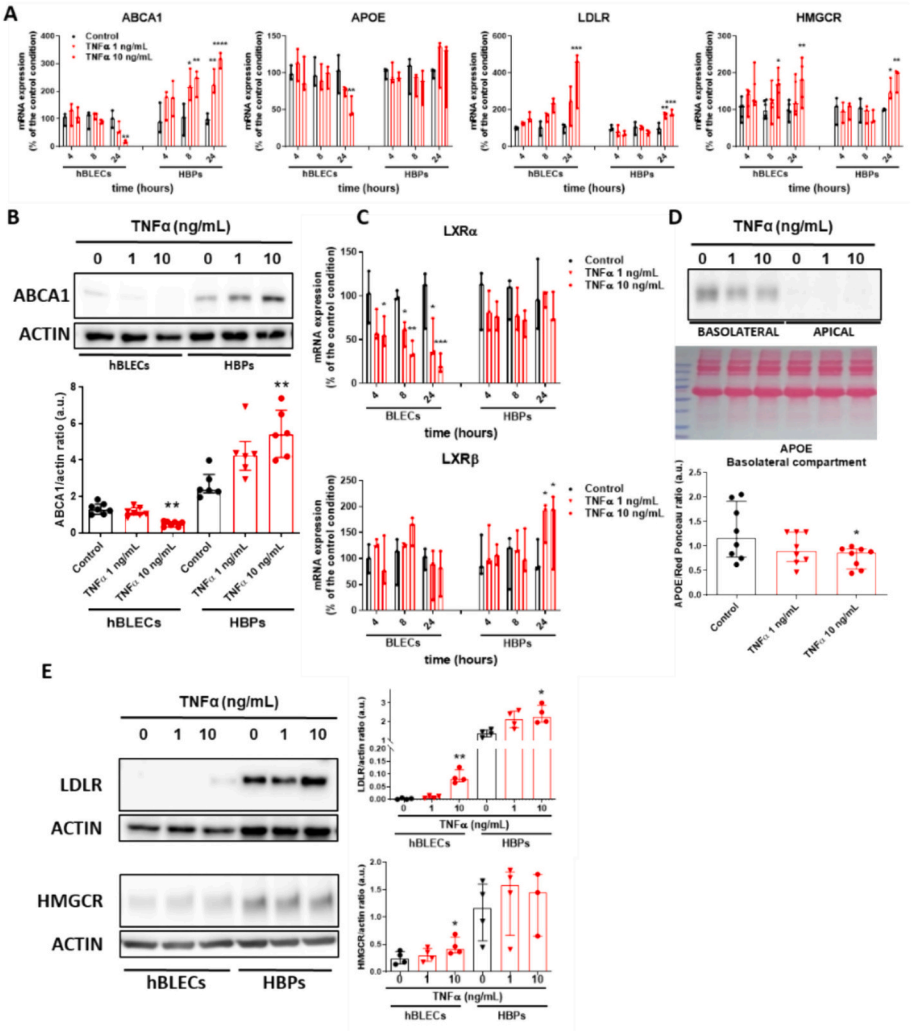

Fig. 4. Time- and concentration-dependent effects of TNFα on the expression of key players in cellular cholesterol homeostasis. RT–qPCR was performed on cell lysates from an *in vitro* BBB model (hBLECs and HBPs) treated for 4, 8 or 24 h with 1 or 10 ng/mL TNFα to detect the mRNA expression of *ABCA1*, *APOE*, *LDLR* and *HMGCR* (A). The corresponding protein expression levels of ABCA1 (B), secreted APOE (D), LDLR and HMGCR E) were quantified after 24 h of TNFα treatment at 1 and 10 ng/mL. C, *LXRα* and *LXRβ* expression was studied by RT–qPCR. The data are presented as medians with interquartile ranges (n = 3–8).

DHC (CYP7B1). TNFα treatment decreased *CH25H* mRNA (Fig. 6B) in hBLECs but strongly upregulated its expression in HBPs (Fig. 6B). *CYP7B1* expression was not detected in hBLECs but was increased by TNFα in HBPs (Fig. 6B). However, further immunoblot studies did not confirm these increases or decreases and suggested that the protein levels of CH25H and CYP7B1 were not affected by TNFα (Fig. 6C and D).

To further investigate whether TNFα modulates 25-HC production, we determined 25-HC levels by carrying out a LC-MS/MS analysis in hBLEC and HBP lysates, as well as in cell culture supernatants. Once CH25H, which is responsible for 25-HC production, is known to be an interferon γ stimulated gene (50), we first showed that IFNγ upregulates 25-HC production in our BBB model (Supplementary Fig. 5), and then, we included this control in our LC-MS/MS experiments. Fig. 6E and F show that both TNFα and IFNγ increased 25-HC production in both cell types. In addition, 25-HC release was increased in the two cell culture supernatants contained in the two compartments (basolateral and apical) of the human BBB model (Fig. 6G). These data strongly suggest that despite no measurable variations in CH25H and CYP7B1 expression, the levels of 25-HC are upregulated by TNFα.

3.4. 25-HC alleviates the TNFα-mediated BBB disruption

To determine whether 25-HC affects BBB permeability, we pretreated the BBB model with 10 μM 25-HC before TNFα treatment. As shown in Fig. 7A, the pretreatment with 25-HC attenuated TNFα-induced BBB disruption after 24 h of treatment, which further supports the hypothesis that 25-HC has protective effects on the BBB under inflammatory conditions. In addition, Fig. 7B confirms that pretreatment with 25-HC improved the cell border localization of CLAUDIN-5, ZO-1 and VE-CADHERIN, and decreased CLAUDIN-5 localization with RAB7A-positive late endosomes (Fig. 7C), that is further confirmed by a decrease of Pearson's correlation coefficient obtained by confocal analysis (Supplementary Fig. 6).

We also investigated the F-ACTIN expression and localization in hBLECs. TNFα treatment induces a significant change in hBLEC morphology, as highlighted by F-ACTIN labelling that appears stronger. This trend is partially reversed by 25-HC pretreatment (Fig. 7B). Finally, 25-HC pretreatment restored hBLEC survival after TNFα treatment (Fig. 7D) and promoted HBP proliferation, as showed in Fig. 7E. The positive proliferative effect of 25-HC on TNFα-treated HBPs was further confirmed by a metabolic activity test (MTT assay) as well as by proliferative marker Ki-67 incorporation assays (Supplementary Fig. 7A and B, respectively).

To determine whether LXR activation or SREBP-2-inhibition is responsible for the decrease in permeability after 25-HC treatment, we pretreated the human BBB model with T0901317 (an LXR agonist),

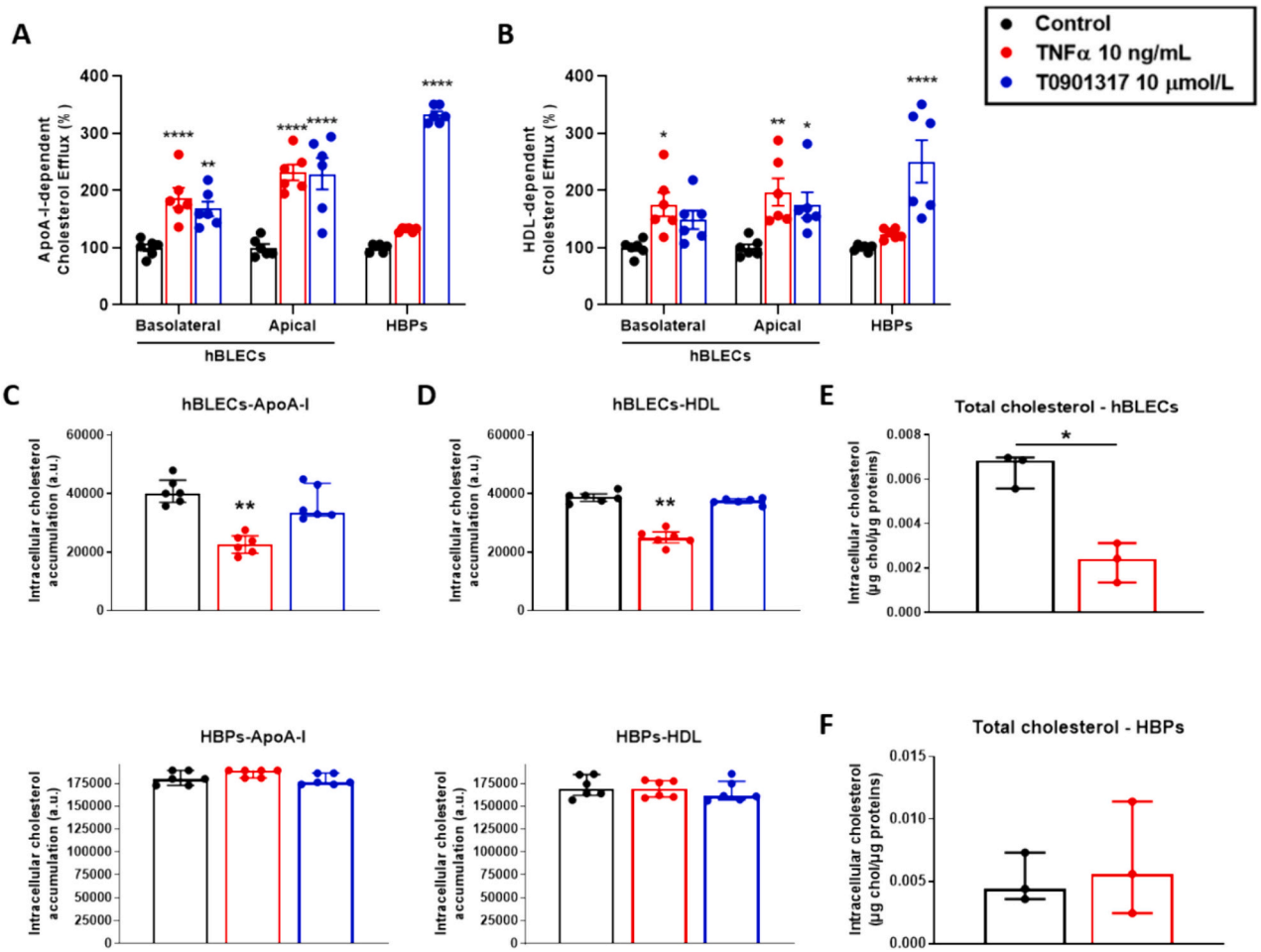

Fig. 5. Effect of 24 h of treatment with TNFα (10 ng/mL) and T0901317 (10 µM) on APOA-I- and HDL-mediated cholesterol efflux by hBLECs and HBPs. T0901317 (10 µM), a potent agonist of the LXR pathway, was used as a positive control. The efflux of cholesterol radiolabeled with the lipid acceptors APOA-I (A) and HDL (B) was determined for 8 h after 24 h of TNFα or T0901317 treatment. The corresponding intracellular cholesterol accumulation is shown in (C), with APOA-I and in (D), with HDL. The data are presented as the medians with interquartile ranges, $n = 6$. Total cholesterol concentration was measured in hBLECs (E) and HBPs (F), as indicated in the material and methods part. The data are presented as the medians with interquartile ranges, $n = 3$.

GSK2033 (an LXR inhibitor) and PF-429242 (that prevents SREBP-2 cleavage by inhibiting the site-1-protease (51)). As shown in Fig. 8, only pretreatment with 25-HC and with SREBP-2 inhibitor partially restored the BBB permeability since there was no significant difference between these 2 conditions and the control condition. We can therefore conclude that the beneficial effect of 25-HC on the TNFα-induced BBB breakdown increase is possibly mediated by SREBP-2 inhibition.

3.5. Cholesterol metabolism is restored by 25-HC pre-treatment

To better understand how 25-HC imbalance could be linked to LXR or SREBP-2 activation under inflammatory conditions, we investigated the effects of 25-HC pretreatment on the levels of key targets associated with both pathways. In this regard, pretreatment with 25-HC partially abolished the TNFα-induced overexpression of LDLR and HMGCR, while it inhibited the TNFα-induced ABCA1 downregulation (Fig. 9). In combination, these results suggest that 25-HC attenuates TNFα-induced LXR downregulation and SREBP-2 activation.

Finally, to determine whether 25-HC has a beneficial effect on the general inflammatory response, we evaluated the expression of key markers of inflammation under 25-HC pretreatment conditions. Despite the beneficial effect observed on BBB permeability, 25-HC pretreatment did not alleviate NRLP3, VCAM-1 or COX-2 expression (Supplementary Fig. 8).

4. Discussion

The BBB isolates the brain from the whole body and strictly controls cholesterol exchange between the central nervous system (CNS) and the bloodstream. The brain is the most cholesterol-rich organ of the body, and its metabolism is altered in neurodegenerative disorders (2,9). It is therefore necessary to better characterize the role of the BBB in CNS cholesterol homeostasis, particularly in the inflammatory context, which systematically occurs in these disorders. The aim of our study was thus to better understand the role of the inflammatory stimulus tumor necrosis factor α (TNFα) on BBB permeability and cholesterol homeostasis using a human *in vitro* model. This model is composed of human endothelial cells derived from hematopoietic stem cells, cocultured with human brain pericytes (HBPs). Endothelial cells then acquire a BBB phenotype, as previously described (32,39), are named human brain-like endothelial cells (hBLECs), and is used to study molecular pathways involved in inflammation and lipid metabolism (34,52,53). In turn, we also previously reported that hBLECs modulate HBP physiology, particularly cholesterol metabolism (41). This model thus represents a unique opportunity to simultaneously investigate the effects of TNFα on different cell types involved in the BBB, as well as to understand better the crosstalk between HBPs and hBLECs in the course of inflammation.

Our results suggest that, when added to the basolateral compartment of the human BBB model, TNFα quickly triggers an inflammatory response in HBPs and hBLECs *via* the activation of the inflammasome

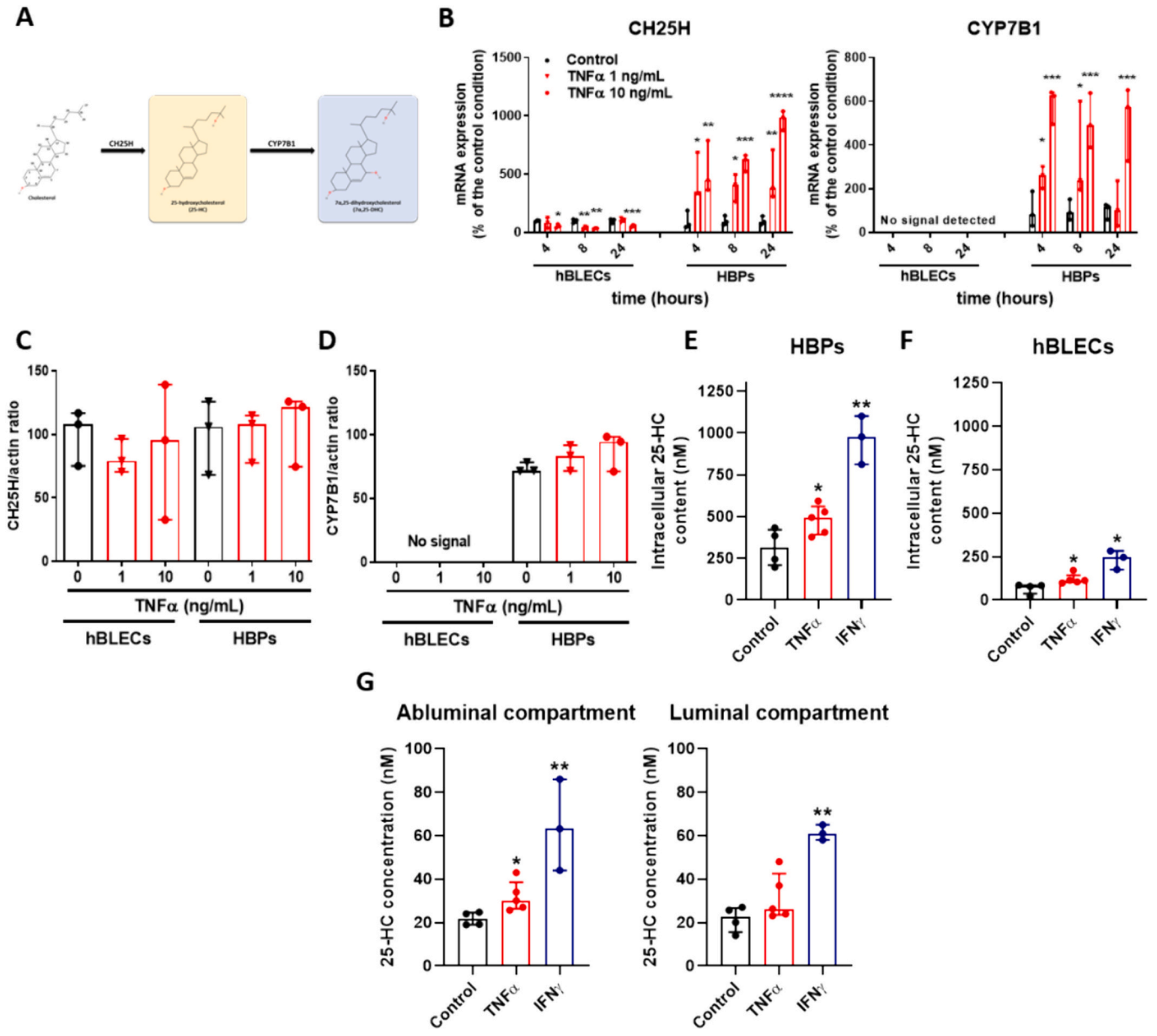

Fig. 6. Effects of TNFα and IFNγ on 25-HC production. (A) Schematic of 25-HC metabolism. Cholesterol is converted into 25-HC by the 25 hydroxylase (CH25H) enzyme located in the endoplasmic reticulum. 25-HC is subsequently converted into 7α,25-dihydroxycholesterol (7α,25-DHC) by the cytochrome P450 family 7 subfamily B member 1 (CYP7B1) enzyme. The effects of TNFα and IFNγ on the mRNA and protein levels of CH25H (B and C) and CYP7B1 (B and D) were determined by RT–qPCR in hBLECs and HBPs. Intracellular 25-HC production in HBPs (E) and in hBLECs (F) after TNFα and IFNγ treatments was measured by LC–MS/MS. (G) 25-HC levels were also quantified in the medium of the BBB model. The data are presented as medians with interquartile ranges (n = 3–5).

protein NLRP3, followed by the upregulation of ICAM-1 and VCAM-1, adhesion molecules that play a key role in immune cell infiltration. At the highest tested dose (10 ng/mL), TNFα did not affect HBP viability but provoked a slight decrease in BLEC viability. TNFα dose-dependently increases BBB permeability by modulating hBLEC tight junctions, as recently suggested (34,52). However, these studies suggest a decrease of CLAUDIN-5 localization at the cell border after a TNFα treatment but did not further investigate this mechanism. In this work, we observed that the tight junction protein CLAUDIN-5 moves, after TNFα treatment, in an intracellular compartment expressing the late endosomal markers (RAB7A). It has been demonstrated that RAB7A-positive late endosomes are able to fuse with lysosomes (48), and we report a decrease in CLDN5 expression in TNFα-treated cells. Taken together, these results suggest that CLAUDIN-5 is relocalized from the cell border to late endosomes and subsequently degraded, thus explaining the loss of permeability observed after TNFα treatment. TNFα treatment also changes the hBLEC morphology, as observed with the ACTIN labelling. This effect was already reported after organophosphorous component (OPs) exposition (54). OPs are toxic molecules used as pesticides or as warfare nerve agents, and toxicological effects of OPs on BBB permeability and cell survival were previously reported in the literature (54). Authors have investigated hBLEC morphological changes after OPs treatment and suggested that it may be attributed to a morphological coping mechanism for preventing the formation of meaningful intercellular gaps and maintaining barrier integrity. We can therefore suggest that the morphological changes observed in our experiments, after TNFα exposition, is a cellular mechanism that would help to compensate the cell loss and would allow to avoid a total barrier disruption.

TNFα also strongly affects cellular cholesterol homeostasis in hBLECs

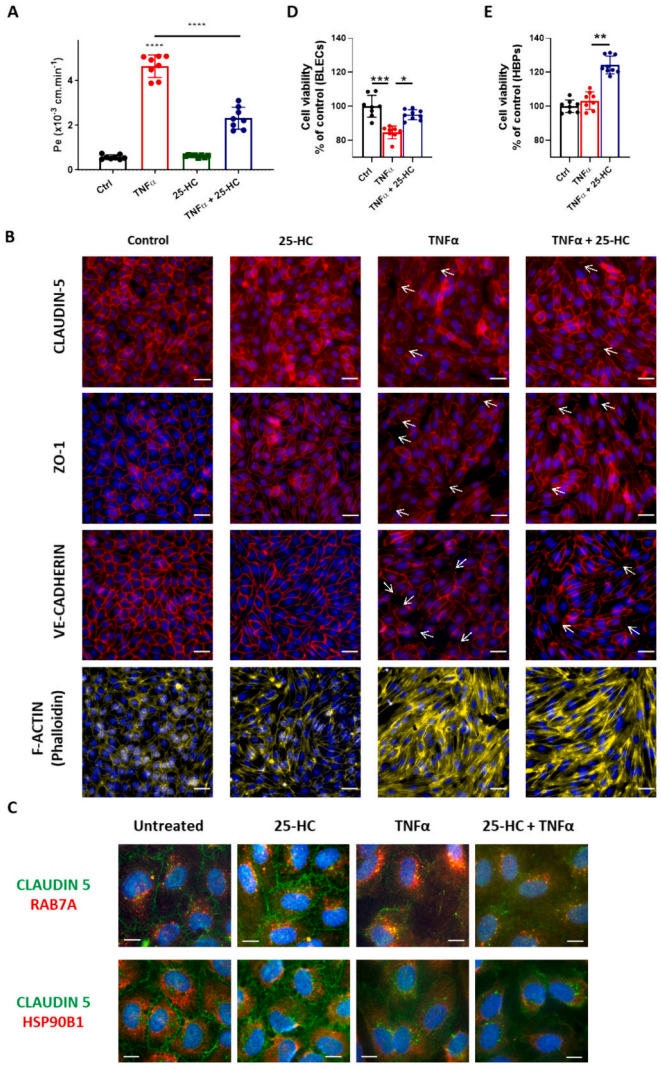

Fig. 7. Effect of 25-HC pretreatment on TNFα-induced BBB disruption. *In vitro* BBB model mice were pretreated with 25-HC (10 μM) for 15 min and then treated with TNFα (10 ng/mL) for 24 h. 25-HC alleviates the increase in paracellular permeability induced by TNFα (A). (B) The immunofluorescence localization of the tight junction (associated) proteins CLAUDIN-5 and ZO-1 and the adherens junction proteins VE-CADHERIN and F-ACTIN (phalloidin staining, yellow) was assessed in hBLECs after 24 h of treatment with DMSO (vehicle, 25-HC, control condition), 10 μM 25-HC, 10 ng/mL TNFα or 10 μM 25-HC + 10 ng/mL TNFα. Nuclei were stained with 10 ng/mL DAPI (blue). Discontinuities in junction protein cell periphery labeling are highlighted by arrows. The pictures are representative of three independent experiments. Scale bar: 20 μm. (C) The immunofluorescence protocol was adapted as described in the Materials and Methods section to specifically study the intracellular location of CLAUDIN-5. TNFα treatment promoted the localization of CLAUDIN-5 in RAB7A-positive late endosomes, but not in endoplasmic reticulum labeled with HSP90B1. Pretreatment of hBLECs with 25-HC decreased this colocalization. Scale bar: 2.5 μm. 25-HC also alleviated the toxicological effects of TNFα on hBLECs (D) and promoted HBP viability (E). The results are presented as medians with interquartile ranges, $n = 8$. (For interpretation of the references to colour in this figure legend, the reader is referred to the web version of this article.)

and HBPs *via* different mechanisms. Indeed, whereas the intracellular cholesterol content was significantly affected in hBLECs, no changes were detected in HBPs. In addition, the expression of ABCA1, which is the major cholesterol efflux transporter, is increased in HBPs but decreased in hBLECs. However, cholesterol efflux to APOA-I and HDL is promoted only in hBLECs. These results support the hypothesis

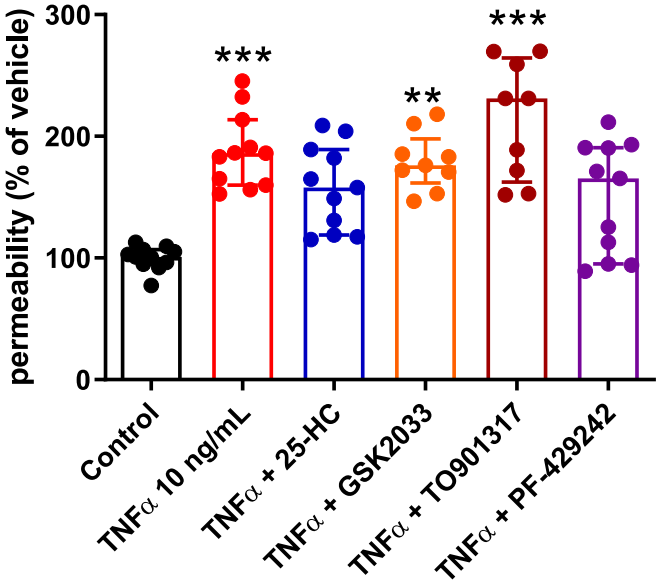

Fig. 8. Effect of LXR and SREBP-2 regulation on TNFα-induced BBB breakdown. Cells were pretreated with GSK2033 (an LXR inhibitor), T0901317 (an LXR agonist), or PF-429242 (a SREBP-2 inhibitor) 15 min prior to TNFα treatment. NaFlu permeability was measured after 24 h of treatment. The data are presented as the medians with interquartile ranges ($n = 11$) and results are compared to the control condition.

suggesting that TNFα-mediated cholesterol efflux is not mediated by ABCA1. Recent studies reported the same observations in red blood cells (55) or in solocultured HBPs since ABCA1-inhibition was not able to decrease cholesterol efflux after TNFα treatment (18). However, whether another transporter is involved remains to be determined. Another possible explanation is that cholesterol diffusion to apolipoproteins or lipoproteins might be a passive mechanism that does not require the involvement of a transporter, as suggested by Lee et al. (56). In all cases, this cholesterol release to APOA-I and HDL might display anti-inflammatory and antioxidative properties, as reported in periphery (57,58). The role of ABCA1 on cholesterol metabolism at the BBB level in the inflammatory context needs further investigation because this transporter is upregulated in HBPs but downregulated in hBLECs and is ultimately not involved in cholesterol efflux processes.

In addition, we observed that TNFα treatment increases the expression of LDLR and possibly promotes cholesterol production by hBLECs *via* upregulation of the enzyme HMGCR. These upregulations might compensate for the exacerbated cholesterol efflux, which possibly leads to a decrease in the intracellular concentration, particularly in hBLECs. Since LDLR and HMGCR are regulated by the SREBP-2 pathway, we may conclude that TNFα-induced inflammation activates this signaling pathway. Taken together, these findings support a major role for cholesterol in the response to inflammation triggered by TNFα *via* the SREBP-2 pathway in both cell types.

Several recent studies revealed changes in oxysterol levels in patients and in animal models mimicking human brain neurodegenerative disorders. In particular, 25-hydroxycholesterol (25-HC) is a cholesterol metabolite that is mainly produced during inflammatory or infectious situations and that in turn contributes to the immune response, CNS disorders, atherosclerosis, macular degeneration, and cancer development (26). In multiple sclerosis (MS) patients, a demyelinating disease, BBB breakdown is reported, and 25-HC levels are altered in CSF and in plasma (27,28). In a mouse model of MS, the experimental autoimmune encephalomyelitis (EAE) model, the levels of *Ch25h*, 25-HC, and 7α,25-DHC are increased in the CNS (59,60), including at the level of the endothelial cells composing the BBB (61). We therefore investigated the effects of TNFα on the mRNA and protein levels of CH25H and CYP71,

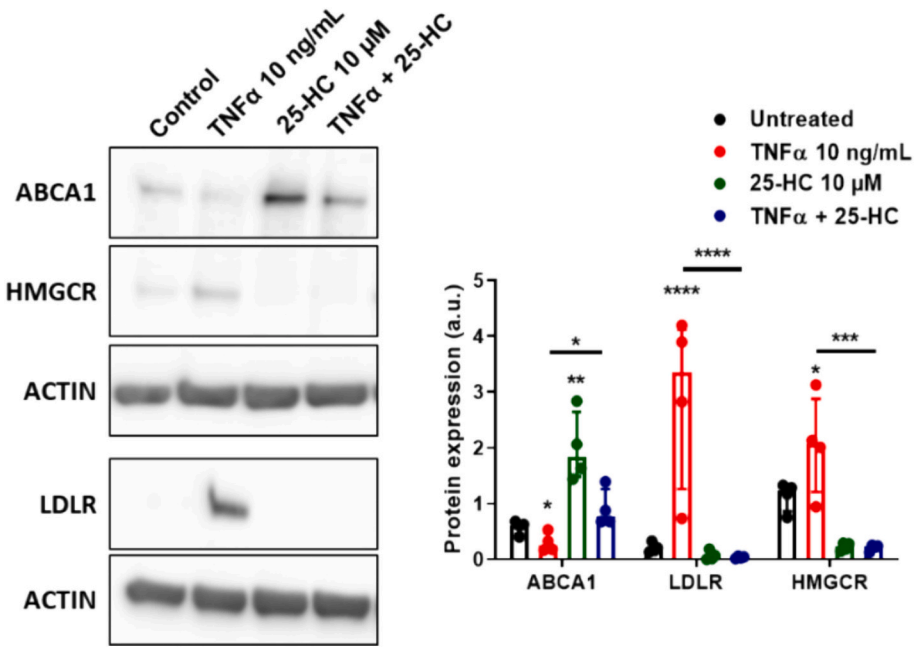

Fig. 9. 25-HC mitigates the effect of TNFα on hBLEC cholesterol metabolism. Pretreatment of hBLECs with 25-HC reduces the effects of TNFα on the protein expression of ABCA1, LDLR and HMGCR. The data are presented as medians with interquartile ranges ($n = 4$) and were compared with the control and TNFα-treated conditions.

which are responsible for conversion of cholesterol to 25-HC and its subsequent metabolization to 7α,25-DHC, respectively. We observed that *CYP7B1* is expressed only by HBPs and not by hBLECs and that its expression is significantly increased after TNFα treatment. TNFα also provoked a decrease in *CH25H* expression in hBLECs but an increase in HBPs. However, these transcriptional modifications were not confirmed at the protein level at 24 h suggesting that other transcriptional or translational mechanisms could be involved in CYP7B1 and CH25H expression. Another possible explanation is that, after 24 h of TNFα treatment, CYP7B1 and CH25H protein expression levels were retourned to their basal levels, as previously reported in LPS-treated mouse astrocytes (62).

Afterwards, detection of 25-HC in the cell culture supernatant and in the cell lysates by mass spectrometry demonstrated that 25-HC levels are markedly increased in both cell types after TNFα treatment. Notably, we also assessed the 7α,25-DHC levels, but we were not able to detect this lipid with or without TNFα treatment. Again, differences in lipid metabolism between HBPs and hBLECs are underlined since basal 25-HC production in HBPs is 7.5-fold greater than that in hBLECs. These results confirm that inflammation modulates 25-HC production, as already reported in other neural cells (59), but to our knowledge, this is the first time that oxysterol production has been directly observed in BBB human cells.

The effects of 25-HC on CNS are not well elucidated so far, with conflicting data on literature. For instance, a study reported a protective role for 25-HC in an EAE mouse model (63), whereas another suggested a deleterious role (60). In addition, Fellows Maxwell et al. measured a 25-HC increase in plasma of progressive MS patients (27), while Crick et al. reported a decrease in relapsing-remitting MS patients (28). To provide further information, we investigated the effects of 25-HC treatment on TNFα-induced inflammation using our human BBB model. When 25-HC was coincubated with TNFα, BBB breakdown was alleviated, cytoskeleton remodeling was attenuated, and CLAUDIN-5 no longer colocalized to late endosomes. In addition, 25-HC pretreatment partially alleviated the effects of TNFα on cholesterol metabolism in hBLECs. Indeed, 25-HC restored the ABCA1 expression, which was downregulated after TNFα treatment. Interestingly, we did not observe ABCA1 upregulation in the presence of 25-HC alone thus suggesting that this oxysterol does not act *via* the canonical LXR signaling pathway as it is observed in other cell types. TNFα strongly upregulates LDLR and HMGCR expression, and we observed that 25-HC impedes this TNFα-dependent upregulation. These data suggest that 25-HC essentially acts *via* the SREBP-2 pathway and not the LXR pathway in hBLECs and HBPs. Indeed, it has been widely described that LDLR and HMGCR expression is regulated by SREBP-2. When the intracellular cholesterol content is high, a constant outflow of cholesterol ensures an increase of this lipid in ER (64). Since CH25H is present in ER, it leads to the conversion of cholesterol into 25-HC (26). Then, this oxysterol production leads to SREBP-2 trapping in the ER, which abolishes LDLR and HMGCR transcription and decreases cholesterol synthesis and uptake (26).

Results of this study are summarized in Fig. 10.

5. Conclusions

Our results suggest that TNFα affects BBB integrity and cholesterol metabolism *via* activation of the SREBP-2 pathway and promotes 25-HC production. In turn, this oxysterol alleviates the effects of TNFα by inhibiting the SREBP-2 pathway. The molecular events leading to the down- and upregulation of ABCA1 expression in hBLECs and HBPs, respectively, remain to be elucidated but likely involve LXRα/LXRβ down- and upregulation. Taken together, our findings suggest that 25-HC may have protective effects at the BBB after TNFα treatment and provides new perspectives for the development of therapeutic approaches to counteract vascular dysfunctions in neuroinflammatory contexts.

Funding

This project was supported by the JPND *PETABC* multinational project (https://pahnkelab.eu/funding/petabc-jpnd/) and was funded by the French National Agency (ANR, #ANR-20-JPW2-0002-04 to F.G.) and Norges Forskningsråd (NFR, #327571 to J.P.). R.A.L. received a fellowship of the *PETABC* project. PETABC is an EU Joint Programme in Neurodegenerative Disease Research (JPND) project. PETABC is supported through the following funding organizations under the aegis of JPND: NFR (Norway; #327571), FFG (Austria; #882717), BMBF

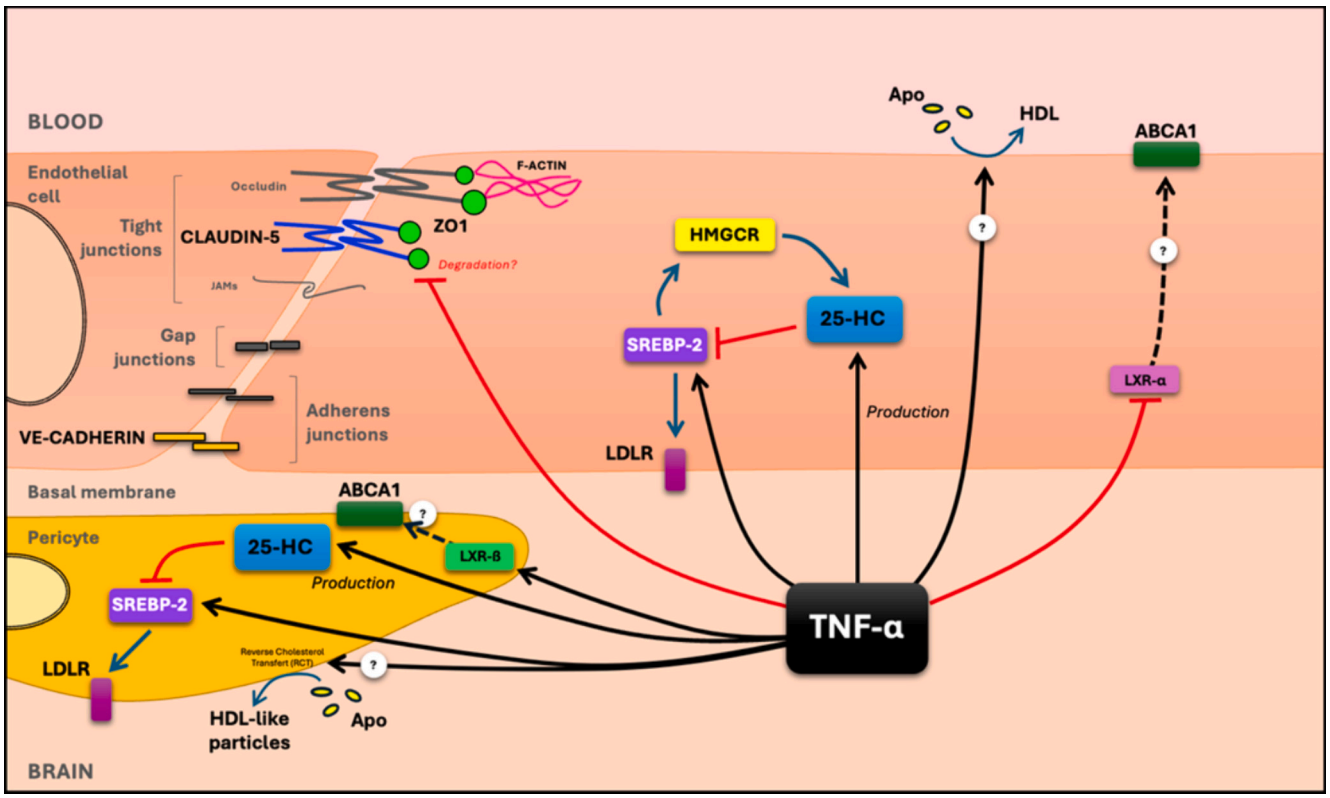

Fig. 10. TNFα promotes the SREBP-2 signaling pathway in hBLECs and HBPs. Using a human BBB model, we demonstrated that TNFα increases BBB permeability by translocating CLAUDIN-5 in RAB7A-positive late endosomes, and by changing hBLEC morphology linked to a strong F-ACTIN remodeling. In parallel, TNFα activates the SREBP-2 pathway, thus leading to upregulation of LDLR and HMGCR expression. ABCA1 expression is increased in HBPs while it is decreased in hBLECs, likely *via* the LXRβ upregulation in HBPs and LXRα downregulation in hBLECs. Despite ABCA1 downregulation in hBLECs, cholesterol release is promoted thus suggesting that this process is ABCA1-independent, and that it might be involved in the inflammatory response as recently suggested in other cell types (18). TNFα also promotes 25-HC production that in turn alleviates the TNFα effects on the BBB permeability and on the cholesterol metabolism.

(Germany; #01ED2106); MSMT (Czech Republic; #8F21002), Latvia; #ES RTD/2020/26, ANR (France; #20-JPW2-0002-04), SRC (Sweden; #2020-02905).

J.S.P received funding from the French National Research Agency (#ANR-21-CE14-0002). F.G. received further funding from the French State and Region Hauts-de-France as part of the CPER 2021-2027 MOSOPS project. S.D. received a fellowship from "Conseil Régional des Hauts-de-France". J.P. received funding from the German Research Foundation (DFG, Germany; #263024513), HelseSØ (Norway; #2019055, #2022046), Barnekreftforeningen (Norway; #19008), EEA and Norway grants Kappa programme (Iceland, Liechtenstein, Norway, Czech Republic; #TO01000078 (TAČR, TARIMAD)), Norges Forskningsråd (NFR, Norway; #295910 (NAPI), #327571 (PETABC)). The *Norwegian Advance Proteomics Infrastructure* (NAPI, www.napi.uio.no) is a National Infrastructure Initiative.

The mass spectrometer of the Spectrométrie de Masse de l'Artois (SMART) facilities used in this study was funded by the European Regional Development Fund (ERDF), the Hauts-de-France regional council, and the Université d'Artois (France). C.P. received funding from Swiss National Science Foundation (# 310030-192738).

Ethics approval and consent to participate

To generate the HBPs, the study protocol for human tissue was approved by the ethics committee of the Medical Faculty (IRB#: H18–033-6), University of Yamaguchi Graduate School, and was conducted in accordance with the Declaration of Helsinki, as amended in Somerset West in 1996. For the $CD34^{+}$-hematopoietic stem cells, written informed consent was obtained from the family of the participant before enrollment in the study. The collection of human umbilical cord blood requires that infants' parents signed consent forms in compliance with French legislation. The protocol was approved by the French Ministry of Higher Education and Research (CODECOH, Number DC2011-1321). According to French legislation, human cells were handled in the laboratory under agreement number L2-1235.

CRediT authorship contribution statement

Rodrigo Azevedo Loiola: Writing – review & editing, Writing – original draft, Methodology, Investigation, Formal analysis, Data curation, Conceptualization. **Cindy Nguyen:** Writing – review & editing, Methodology, Formal analysis, Data curation. **Shiraz Dib:** Writing – review & editing, Formal analysis, Data curation. **Julien Saint-Pol:** Writing – review & editing, Methodology, Formal analysis, Data curation. **Lucie Dehouck:** Writing – review & editing, Methodology, Formal analysis. **Emmanuel Sevin:** Writing – review & editing, Methodology, Formal analysis. **Marie Naudot:** Methodology, Formal analysis. **Christophe Landry:** Writing – review & editing, Methodology, Formal analysis. **Jens Pahnke:** Writing – review & editing, Resources, Methodology, Funding acquisition. **Caroline Pot:** Writing – review & editing, Resources, Methodology. **Fabien Gosselet:** Writing – review & editing, Writing – original draft, Supervision, Project administration, Funding acquisition, Formal analysis, Data curation, Conceptualization.

Declaration of competing interest

The authors declare that they have no known competing financial interests or personal relationships that could have appeared to influence the work reported in this paper.

Data availability

Data will be made available on request.

References

[1] J.M. Dietschy, S.D. Turley, Thematic review series: brain lipids. Cholesterol metabolism in the central nervous system during early development and in the mature animal, J. Lipid Res. 45 (8) (2004) 1375–1397.
[2] M.G. Martín, F. Pfrieger, C.G. Dotti, Cholesterol in brain disease: sometimes determinant and frequently implicated, EMBO Rep. 15 (10) (2014) 1036–1052.
[3] F. Gosselet, J. Saint-Pol, L. Fenart, Effects of Oxysterols on the Blood-Brain Barrier: Implications for Alzheimer's Disease, Biochem Biophys Res Commun, 2014.
[4] N.J. Abbott, A.A. Patabendige, D.E. Dolman, S.R. Yusof, D.J. Begley, Structure and function of the blood-brain barrier, Neurobiol. Dis. 37 (1) (2010) 13–25.
[5] F. Gosselet, R.A. Loiola, A. Roig, A. Rosell, M. Culot, Central nervous system delivery of molecules across the blood-brain barrier, Neurochem. Int. 104952 (2021).
[6] R. Cecchelli, V. Berezowski, S. Lundquist, M. Culot, M. Renftel, M.P. Dehouck, et al., Modelling of the blood-brain barrier in drug discovery and development, Nat. Rev. Drug Discov. 6 (8) (2007) 650–661.
[7] C. Menaceur, F. Gosselet, L. Fenart, J. Saint-Pol, The blood-brain barrier, an evolving concept based on technological advances and cell-cell communications, Cells 11 (1) (2021).
[8] I.J. Martins, T. Berger, M.J. Sharman, G. Verdile, S.J. Fuller, R.N. Martins, Cholesterol metabolism and transport in the pathogenesis of Alzheimer's disease, J. Neurochem. 111 (6) (2009) 1275–1308.
[9] Y. Gao, S. Ye, Y. Tang, W. Tong, S. Sun, Brain cholesterol homeostasis and its association with neurodegenerative diseases, Neurochem. Int. 171 (2023) 105635.
[10] A. Zarrouk, M. Debbabi, M. Bezine, E.M. Karym, A. Badreddine, O. Rouaud, et al., Lipid biomarkers in Alzheimer's disease, Curr. Alzheimer Res. 15 (4) (2018) 303–312.
[11] R. Koldamova, M. Staufenbiel, I. Lefterov, Lack of ABCA1 considerably decreases brain ApoE level and increases amyloid deposition in APP23 mice, J. Biol. Chem. 280 (52) (2005) 43224–43235.
[12] S.E. Wahrle, H. Jiang, M. Parsadanian, R.E. Hartman, K.R. Bales, S.M. Paul, et al., Deletion of Abca1 increases Abeta deposition in the PDAPP transgenic mouse model of Alzheimer disease, J. Biol. Chem. 280 (52) (2005) 43236–43242.
[13] S.E. Wahrle, H. Jiang, M. Parsadanian, J. Kim, A. Li, A. Knoten, et al., Overexpression of ABCA1 reduces amyloid deposition in the PDAPP mouse model of Alzheimer disease, J. Clin. Invest. 118 (2) (2008) 671–682.
[14] H. Holstege, M. Hulsman, C. Charbonnier, B. Grenier-Boley, O. Quenez, D. Grozeva, et al., Exome sequencing identifies rare damaging variants in ATP8B4 and ABCA1 as risk factors for Alzheimer's disease, Nat. Genet. 54 (12) (2022) 1786–1794.
[15] P. Costet, Y. Luo, N. Wang, A.R. Tall, Sterol-dependent transactivation of the ABC1 promoter by the liver X receptor/retinoid X receptor, J. Biol. Chem. 275 (36) (2000) 28240–28245.
[16] R. Koldamova, N.F. Fitz, I. Lefterov, The role of ATP-binding cassette transporter A1 in Alzheimer's disease and neurodegeneration, Biochim. Biophys. Acta 1801 (8) (2010) 824–830.
[17] J. Saint-Pol, P. Candela, M.C. Boucau, L. Fenart, F. Gosselet, Oxysterols decrease apical-to-basolateral transport of Abeta peptides via an ABCB1-mediated process in an in vitro blood-brain barrier model constituted of bovine brain capillary endothelial cells, Brain Res. 1517 (2013) 1–15.
[18] S. Dib, R.A. Loiola, E. Sevin, J. Saint-Pol, F. Shimizu, T. Kanda, et al., TNFα activates the liver X receptor signaling pathway and promotes cholesterol efflux from human brain Pericytes independently of ABCA1, Int. J. Mol. Sci. 24 (6) (2023).
[19] U. Panzenboeck, Z. Balazs, A. Sovic, A. Hrzenjak, S. Levak-Frank, A. Wintersperger, et al., ABCA1 and scavenger receptor class B, type I, are modulators of reverse sterol transport at an in vitro blood-brain barrier constituted of porcine brain capillary endothelial cells, J. Biol. Chem. 277 (45) (2002) 42781–42789.
[20] J.D. Horton, J.L. Goldstein, M.S. Brown, SREBPs: activators of the complete program of cholesterol and fatty acid synthesis in the liver, J. Clin. Invest. 109 (9) (2002) 1125–1131.
[21] J.D. Horton, N.A. Shah, J.A. Warrington, N.N. Anderson, S.W. Park, M.S. Brown, et al., Combined analysis of oligonucleotide microarray data from transgenic and knockout mice identifies direct SREBP target genes, Proc. Natl. Acad. Sci. USA 100 (21) (2003) 12027–12032.
[22] A. Mazein, S. Watterson, W.Y. Hsieh, W.J. Griffiths, P. Ghazal, A comprehensive machine-readable view of the mammalian cholesterol biosynthesis pathway, Biochem. Pharmacol. 86 (1) (2013) 56–66.
[23] M.S. Brown, J.R. Faust, J.L. Goldstein, Role of the low density lipoprotein receptor in regulating the content of free and esterified cholesterol in human fibroblasts, J. Clin. Invest. 55 (4) (1975) 783–793.
[24] V. Mutemberezi, O. Guillemot-Legris, G.G. Muccioli, Oxysterols: from cholesterol metabolites to key mediators, Prog. Lipid Res. 64 (2016) 152–169.
[25] G. Testa, E. Staurenghi, C. Zerbinati, S. Gargiulo, L. Iuliano, G. Giaccone, et al., Changes in brain oxysterols at different stages of Alzheimer's disease: their involvement in neuroinflammation, Redox Biol. 10 (2016) 24–33.
[26] C. Nguyen, J. Saint-Pol, S. Dib, C. Pot, F. Gosselet, 25-Hydroxycholesterol in health and diseases, J. Lipid Res. 65 (1) (2024) 100486.
[27] K. Fellows Maxwell, S. Bhattacharya, M.L. Bodziak, D. Jakimovski, J. Hagemeier, R.W. Browne, et al., Oxysterols and apolipoproteins in multiple sclerosis: a 5 year follow-up study, J. Lipid Res. 60 (7) (2019) 1190–1198.
[28] P.J. Crick, W.J. Griffiths, J. Zhang, M. Beibel, J. Abdel-Khalik, J. Kuhle, et al., Reduced plasma levels of 25-hydroxycholesterol and increased cerebrospinal fluid levels of bile acid precursors in multiple sclerosis patients, Mol. Neurobiol. 54 (10) (2017) 8009–8020.
[29] D. Meffre, G. Shackleford, M. Hichor, V. Gorgievski, E.T. Tzavara, A. Trousson, et al., Liver X receptors alpha and beta promote myelination and remyelination in the cerebellum, Proc. Natl. Acad. Sci. USA 112 (24) (2015) 7587–7592.
[30] M.Y. Wong, M. Lewis, J.J. Doherty, Y. Shi, A.G. Cashikar, A. Amelianchik, et al., 25-Hydroxycholesterol amplifies microglial IL-1β production in an apoE isoform-dependent manner, J. Neuroinflammation 17 (1) (2020) 192.
[31] I.H.K. Dias, H. Shokr, F. Shephard, L. Chakrabarti, Oxysterols and oxysterol sulfates in Alzheimer's disease brain and cerebrospinal fluid, J. Alzheimers Dis. 87 (4) (2022) 1527–1536.
[32] R. Cecchelli, S. Aday, E. Sevin, C. Almeida, M. Culot, L. Dehouck, et al., A stable and reproducible human blood-brain barrier model derived from hematopoietic stem cells, PLoS One 9 (6) (2014) e99733.
[33] C. Bellenguez, F. Küçükali, I.E. Jansen, L. Kleineidam, S. Moreno-Grau, N. Amin, et al., New insights into the genetic etiology of Alzheimer's disease and related dementias, Nat. Genet. 54 (4) (2022) 412–436.
[34] G.H.O. da Rocha, R.A. Loiola, M. de Paula-Silva, F. Shimizu, T. Kanda, A. Vieira, et al., Pioglitazone attenuates the effects of peripheral inflammation in a human in vitro blood-brain barrier model, Int. J. Mol. Sci. 23 (21) (2022).
[35] R. Versele, M. Corsi, A. Fuso, E. Sevin, R. Businaro, F. Gosselet, et al., Ketone bodies promote amyloid-beta1-40 clearance in a human in vitro blood-brain barrier model, Int. J. Mol. Sci. 21 (3) (2020).
[36] F. Shimizu, Y. Sano, M.A. Abe, T. Maeda, S. Ohtsuki, T. Terasaki, et al., Peripheral nerve pericytes modify the blood-nerve barrier function and tight junctional molecules through the secretion of various soluble factors, J. Cell. Physiol. 226 (1) (2011) 255–266.
[37] D.C. Pedroso, A. Tellechea, L. Moura, I. Fidalgo-Carvalho, J. Duarte, E. Carvalho, et al., Improved survival, vascular differentiation and wound healing potential of stem cells co-cultured with endothelial cells, PLoS One 6 (1) (2011) e16114.
[38] C. Deligne, J. Hachani, S. Duban-Deweer, S. Meignan, P. Leblond, A.M. Carcaboso, et al., Development of a human in vitro blood-brain tumor barrier model of diffuse intrinsic pontine glioma to better understand the chemoresistance, Fluids Barriers CNS 17 (1) (2020) 37.
[39] M.P. Dehouck, M. Tachikawa, Y. Hoshi, K. Omori, C.A. Maurage, G. Strecker, et al., Quantitative targeted absolute proteomics for better characterization of an in vitro human blood-brain barrier model derived from hematopoietic stem cells, Cells 11 (24) (2022).
[40] M. Heymans, R. Figueiredo, L. Dehouck, D. Francisco, Y. Sano, F. Shimizu, et al., Contribution of brain pericytes in blood-brain barrier formation and maintenance: a transcriptomic study of cocultured human endothelial cells derived from hematopoietic stem cells, Fluids Barriers CNS 17 (1) (2020) 48.
[41] C. Menaceur, J. Hachani, S. Dib, S. Duban-Deweer, Y. Karamanos, F. Shimizu, et al., Highlighting in vitro the role of brain-like endothelial cells on the maturation and metabolism of brain Pericytes by SWATH proteomics, Cells 12 (7) (2023).
[42] M.P. Dehouck, P. Jolliet-Riant, F. Bree, J.C. Fruchart, R. Cecchelli, J.P. Tillement, Drug transfer across the blood-brain barrier: correlation between in vitro and in vivo models, J. Neurochem. 58 (5) (1992) 1790–1797.
[43] A. Limonciel, L. Aschauer, A. Wilmes, S. Prajczer, M.O. Leonard, W. Pfaller, et al., Lactate is an ideal non-invasive marker for evaluating temporal alterations in cell stress and toxicity in repeat dose testing regimes, Toxicol. in Vitro 25 (8) (2011) 1855–1862.
[44] Y. Lamartiniere, M.C. Boucau, L. Dehouck, M. Krohn, J. Pahnke, P. Candela, et al., ABCA7 downregulation modifies cellular cholesterol homeostasis and decreases amyloid-beta peptide efflux in an in vitro model of the blood-brain barrier, J. Alzheimers Dis. 64 (4) (2018) 1195–1211.
[45] E.G. Bligh, W.J. Dyer, A rapid method of total lipid extraction and purification, Can. J. Biochem. Physiol. 37 (8) (1959) 911–917.
[46] M. Reinicke, J. Schröter, D. Müller-Klieser, C. Helmschrodt, U. Ceglarek, Free oxysterols and bile acids including conjugates - simultaneous quantification in human plasma and cerebrospinal fluid by liquid chromatography-tandem mass spectrometry, Anal. Chim. Acta 1037 (2018) 245–255.
[47] Y. Hashimoto, C. Greene, A. Munnich, M. Campbell, The CLDN5 gene at the blood-brain barrier in health and disease, Fluids Barriers CNS 20 (1) (2023) 22.
[48] Y.B. Hu, E.B. Dammer, R.J. Ren, G. Wang, The endosomal-lysosomal system: from acidification and cargo sorting to neurodegeneration, Transl. Neurodegener. 4 (2015) 18.
[49] J. Saint-Pol, E. Vandenhaute, M.C. Boucau, P. Candela, L. Dehouck, R. Cecchelli, et al., Brain pericytes ABCA1 expression mediates cholesterol efflux but not cellular amyloid-beta peptide accumulation, J. Alzheimers Dis. 30 (3) (2012) 489–503.
[50] K. Park, A.L. Scott, Cholesterol 25-hydroxylase production by dendritic cells and macrophages is regulated by type I interferons, J. Leukoc. Biol. 88 (6) (2010) 1081–1087.

[51] J.W.M. Fowler, R. Zhang, B. Tao, N.E. Boutagy, W.C. Sessa, Inflammatory stress signaling via NF-kB alters accessible cholesterol to upregulate SREBP2 transcriptional activity in endothelial cells, eLife 11 (2022).
[52] R. Versele, E. Sevin, F. Gosselet, L. Fenart, P. Candela, TNF-α and IL-1β modulate blood-brain barrier permeability and decrease amyloid-β peptide efflux in a human blood-brain barrier model, Int. J. Mol. Sci. 23 (18) (2022).
[53] M. Kuntz, P. Candela, J. Saint-Pol, Y. Lamartiniere, M.C. Boucau, E. Sevin, et al., Bexarotene promotes cholesterol efflux and restricts apical-to-basolateral transport of amyloid-beta peptides in an in vitro model of the human blood-brain barrier, J. Alzheimers Dis. 48 (3) (2015) 849–862.
[54] N.J. Abbott, C.C. Hughes, P.A. Revest, J. Greenwood, Development and characterisation of a rat brain capillary endothelial culture: towards an in vitro blood-brain barrier, J. Cell Sci. 103 (Pt 1) (1992) 23–37.
[55] R. Ohkawa, H. Low, N. Mukhamedova, Y. Fu, S.J. Lai, M. Sasaoka, et al., Cholesterol transport between red blood cells and lipoproteins contributes to cholesterol metabolism in blood, J. Lipid Res. 61 (12) (2020) 1577–1588.
[56] M.S. Lee, S.J. Bensinger, Reprogramming cholesterol metabolism in macrophages and its role in host defense against cholesterol-dependent cytolysins, Cell. Mol. Immunol. 19 (3) (2022) 327–336.
[57] P. Fotakis, V. Kothari, D.G. Thomas, M. Westerterp, M.M. Molusky, E. Altin, et al., Anti-inflammatory effects of HDL (high-density lipoprotein) in macrophages predominate over proinflammatory effects in atherosclerotic plaques, Arterioscler. Thromb. Vasc. Biol. 39 (12) (2019) e253–e272.
[58] E. Grao-Cruces, S. Lopez-Enriquez, M.E. Martin, S. Montserrat-de la Paz, High-density lipoproteins and immune response: a review, Int. J. Biol. Macromol. 195 (2022) 117–123.
[59] V. Mutemberezi, B. Buisseret, J. Masquelier, O. Guillemot-Legris, M. Alhouayek, G. G. Muccioli, Oxysterol levels and metabolism in the course of neuroinflammation: insights from in vitro and in vivo models, J. Neuroinflammation 15 (1) (2018) 74.
[60] F. Chalmin, V. Rochemont, C. Lippens, A. Clottu, A.W. Sailer, D. Merkler, et al., Oxysterols regulate encephalitogenic CD4(+) T cell trafficking during central nervous system autoimmunity, J. Autoimmun. 56 (2015) 45–55.
[61] F. Ruiz, B. Peter, J. Rebeaud, S. Vigne, V. Bressoud, M. Roumain, et al., Endothelial cell-derived oxysterol ablation attenuates experimental autoimmune encephalomyelitis, EMBO Rep. 24 (3) (2023) e55328.
[62] A. Rutkowska, S.A. O'Sullivan, I. Christen, J. Zhang, A.W. Sailer, K.K. Dev, The EBI2 signalling pathway plays a role in cellular crosstalk between astrocytes and macrophages, Sci. Rep. 6 (2016) 25520.
[63] A. Reboldi, E.V. Dang, J.G. McDonald, G. Liang, D.W. Russell, J.G. Cyster, Inflammation. 25-hydroxycholesterol suppresses interleukin-1-driven inflammation downstream of type I interferon, Science 345 (6197) (2014) 679–684.
[64] J. Sandhu, S. Li, L. Fairall, S.G. Pfisterer, J.E. Gurnett, X. Xiao, et al., Aster proteins facilitate nonvesicular plasma membrane to ER cholesterol transport in mammalian cells, Cell 175 (2) (2018) 514–529.e520.